CONFÉRENCIERS

P. Armbruster
G.F. Bertsch
J.-P. Blaizot
X. Campi
B. Desplanques
A.H. Mueller
U. Mosel
B. Mottelson
P. Paul
C.J. Pethick
B. Pire
P. Radvanyi
C. Rubbia
R.H. Siemssen
G. Sletten
M. Spiro
B. Tamain
S. Vervier
W. Weise

UJFG

LES HOUCHES

SESSION LXVI

30 Juillet – 30 Août 1996

OÙ EN EST LA PHYSIQUE NUCLÉAIRE APRÈS 100 ANS D'EXISTENCE ?

TRENDS IN NUCLEAR PHYSICS, 100 YEARS LATER

édité par

H. NIFENECKER, J.-P. BLAIZOT, G.F. BERTSCH
W. WEISE *et* F. DAVID

1998

ELSEVIER
Amsterdam – Lausanne – New York – Oxford – Shannon – Singapore – Tokyo

[33] W. Pauli, Letter to the Tübingen meeting, 4 December 1930, in: *W. Pauli Collected Scientific Papers*, Vol. 2, R. Kronig and V. Weisskopf, Eds. (Interscience, New York, 1964) p. 1313.
[34] E. Fermi, Z. Physik **88** (1934) 161.
[35] I. Curie and F. Joliot, C.R. Acad. Sci. Paris **198** (1934) 254, 559.
[36] F. Reines and C.L. Cowan, Phys. Rev. **92** (1953) 830; C.L. Cowan, F. Reines, F.B. Harrison, H.W. Kruse and A.D. Mc Guire, Science **124** (1956) 103.
[37] G. Gamow, Z. Physik **51** (1928) 204.
[38] J.D. Cockcroft and E.T.S. Walton, Proc. Roy. Soc. **A137** (1932) 229.
[39] E.O. Lawrence and M.S. Livingston, Phys. Rev. **40** (1932) 19.
[40] H. Urey, F.G. Brickwedde and G.M. Murphy, Phys. Rev. **39** (1932) 164, 864.
[41] C.D. Anderson, Science **76** (1932) 238; Phys. Rev. **43** (1933) 491.
[42] W. Bothe and H. Becker, Z. Physik **66** (1930) 289.
[43] I. Curie and F. Joliot, C.R. Acad. Sci. Paris **194** (1932) 273.
[44] J. Chadwick, Nature **129** (1932) 312; Proc. Roy. Soc. **A136** (1932) 692.
[45] W. Heisenberg, Z. Physik **77** (1932) 1; **78** (1932) 156; **80** (1933) 587.
[46] H. Yukawa, Proc. Phys.-Math. Soc. Jpn **17(3)** (1935) 48.
[47] E. Fermi, Nature **133** (1934) 757, 898; E. Fermi, E. Amaldi, O. D'Agostino, F. Rasetti and E. Segré, Proc. Roy. Soc. **A146** (1934) 483.
[48] H.A. Bethe and C.L. Critchfield, Phys. Rev. **54** (1938) 248, 862.
[49] C. von Weiszäcker, Phys. Z. **39** (1938) 633.
[50] H.A. Bethe, Phys. Rev. **55** (1939) 434.
[51] E. Fermi, F. Rasetti and O. D'Agostino, Ricerca Sci. **1** (1934) 542.
[52] I. Curie and P. Savitch, J. Phys. Rad. **9** (1938) 355.
[53] O. Hahn and F. Strassmann, Naturwiss. **27** (1939) 11.
[54] W. Gerlach and D. Hahn, *Otto Hahn* (Wissenschaftliche Verlagsges. Stuttgart, 1984); O.R. Frisch, Physics Today (Nov. 1967) 43.
[55] L. Meitner and O. Frisch, Nature **143** (1939) 239.
[56] O. Frisch, Nature **143** (1939) 276.
[57] F. Joliot, C.R. Acad. Sci. Paris **208** (1939) 341, 647; J. Phys. Rad. **10** (1939) 159.
[58] N. Bohr, Phys. Rev. **55** (1939) 418.
[59] H. von Halban, F. Joliot and L. Kowarski, Nature **143** (1939) 470, 680, 939; M. Dodé, H. von Halban, F. Joliot and L. Kowarski, C.R. Acad. Sci. Paris **208** (1939) 995.
[60] H.L. Anderson, E. Fermi and H.B. Hanstein, Phys. Rev. **55** (1939) 797; L. Szilard and W.H. Zinn, Phys. Rev. **55** (1939) 799.

COURSE 2

ELEMENTARY FEATURES OF NUCLEAR STRUCTURE

B. Mottelson

NORDITA, Blegdamsvej 17, DK-2100 Copenhagen Ø, Denmark

H. Nifenecker, J.-P. Blaizot, G.F. Bertsch, W. Weise and F. David, eds.
Les Houches, Session LXVI, 1996
Où en est la physique nucléaire après 100 ans d'existence?
Trends in Nuclear Physics, 100 Years Later

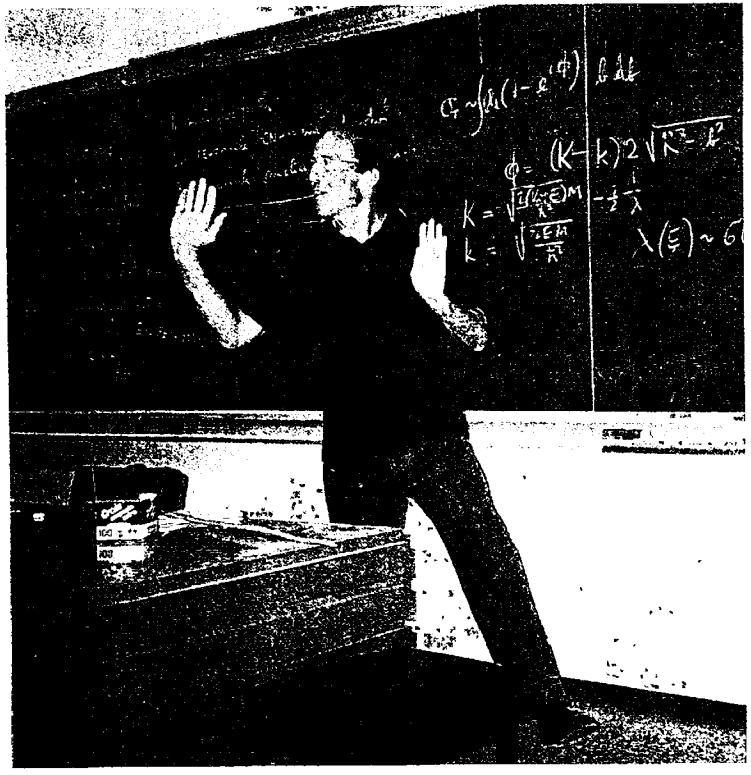

Contents

0. Introduction

The aim of the present lectures is to provide a short presentation of the most elementary features of nuclear structure as revealed in the study of nuclear spectra at low excitation energy. Indeed, the spectra can be seen as a kind of coded message providing our principal source of information concerning the quantal structure of many-body systems; these lectures are thus an introduction to some of the ideas that have been found useful in deciphering this code. The main themes concern independent particle motion, shell structure, pairing, deformation and collective rotation, but I shall begin with a review of some of the spectroscopic evidence for chaotic features in nuclear dynamics.

1. Chaotic structures in nuclear spectra

I take chaotic structures first because it seems to me that one of the important areas that remain poorly understood involves the interface between order and chaos – how should we think about the competition between these two aspects of nuclear structure?; are there cross-over regions in the nuclear spectra that separate different regimes for this competition? These are issues of current debate and important questions that must be kept in mind as we later develop the concepts involved in describing the ordered structures.

Although I shall not present an historical development of most of the themes in these chapters, I cannot resist introducing the topic of chaos in nuclei with a discussion of the historical context of nuclear physics in the mid 1930s when this theme was first introduced by Niels Bohr.

The discovery of artificial radioactivity in 1934 by Frédéric Joliot and Irene Curie opened the possibility of vastly expanding the studies of nuclei. The reaction discovered by the Joliot's involved the bombardment of aluminum by α-particles from polonium ($^{4}_{2}\mathrm{He} + ^{27}_{13}\mathrm{Al} \longrightarrow ^{30}_{15}\mathrm{P} + \mathrm{n}$; $^{30}_{15}\mathrm{P} \longrightarrow ^{30}_{14}\mathrm{Si} + \mathrm{e}^{+}(\tau = 2.5\,\mathrm{min})$). The energies of charged particles available at that time for bombarding nuclei limited such reactions to rather light nuclei since the Coulomb barrier prevented reactions with heavier targets. Thus, the scope of artificial radioactivity was again greatly extended when Fermi and his group took up the study of neutron-induced

radioactivity; the neutron (without charge) could penetrate into and produce reactions with even the heaviest nuclei. Within a few months (in 1935), Fermi's group had discovered almost fifty new radioactivities produced by reactions with neutrons. Next, they began systematic studies of the cross sections for interaction of neutrons with nuclei – how these reactions depended on energy and on target material.

The interpretation of these cross sections provided a challenge for theoretical interpretation, and within less than a year four different groups of investigators published theoretical work on this problem. All of these investigators used essentially the same theoretical approach, which was taken over almost directly from the description that had been successful in interpreting the interactions of electrons with atoms. The neutron was assumed to interact with an average potential produced by the target nucleus; on entering the target it moves back and forth a few times, being reflected by the steep potential at the nuclear surface and then either emits a γ-ray going into a lower energy bound state in the potential or goes out of the nucleus into a final state that corresponds to an elastic scattering. The results of this analysis are so simple to obtain and are of such general importance for the development, that I would like to briefly sketch the qualitative features of the derivation.

We shall focus on the issue of the relative probability for elastic scattering as compared with capture resulting from gamma-ray emission for neutrons with low energies, i.e., in the range of thermal energies, $E_n \sim \frac{1}{40}$ eV, up to a few tens of eV, since it was in this energy range that the experimental measurements were revealing such interesting results. For a neutron bouncing back and forth in the nuclear potential, the rate T^γ of emission of dipole γ-rays is given by the formula, familiar from atomic physics,

$$\mathrm{T}^\gamma \sim \frac{1}{\hbar} D^2 k_\gamma^3, \tag{1.1}$$

where D is the dipole matrix element connecting the initial and final neutron state and k_γ is the wave number of the emitted γ-ray and the factor k_γ^3 is essentially the measure of phase space for the emitted dipole γ-ray. Taking

$$D \sim eR \qquad R = \text{nuclear radius}$$

we obtain

$$\mathrm{T}^\gamma \sim \frac{e^2}{\hbar c} (k_\gamma R)^2 k_\gamma c \tag{1.2}$$

The rate of escape of the neutron from the virtual state in the nucleus depends partly on the transmission coefficient, T, which can be estimated by considering the fractional transmission of a plane wave incident on a one-dimensional step

potential

$$\mathrm{T} = \frac{4k_{in}k_{out}}{(k_{in} + k_{out})^2} \approx \sqrt{\frac{\epsilon_{out}}{\epsilon_F}} \tag{1.3}$$

where k_{in} and k_{out} are the neutron wave numbers on the two sides of the step in the potential, while ϵ_{out} is the neutron energy outside the nucleus ($\sim$ 10 eV in these experiments) and ϵ_F is the kinetic energy of the neutron inside the nucleus ($\sim$ 40 MeV). The rate of escape is equal to the transmission coefficient times the rate of collision with the barrier

$$\mathrm{T}_{escape} = \mathrm{T} \cdot \frac{v_F}{R}$$

So we get

$$\frac{\mathrm{T}^\gamma}{\mathrm{T}_{escape}} \sim \frac{e^2}{\hbar c}(k_\gamma R)^3 \frac{c}{v_F} \sqrt{\frac{\epsilon_F}{\epsilon_{out}}} \sim \frac{1}{10} \tag{1.4}$$

Thus, the theory predicts capture to be somewhat less probable than scattering even in the most favorable cases. It is also a clear prediction of this analysis that any structure in the cross-section (resonance) should have a characteristic scale of energy determined by the frequency of the motions of the neutron in the average nuclear potential

$$\Delta E_{res} \sim \frac{\hbar v_F}{R} \sim 10 \text{ MeV} \tag{1.5}$$

No sooner were these theoretical predictions published than the experiments provided dramatic evidence in contradiction to the theory; the capture was often hundreds or thousands of times more probable than scattering, and striking resonance structure was observed in the cross-sections with characteristic energy spacings almost a million times smaller than the estimate (1.5), (see Fig. 1).

It was Niels Bohr who, pondering over these experiments, recognized first and most clearly that the error of the simple theory resulted from a failure to appreciate the many-body aspects of the neutron reaction process. His new ideas are beautifully recorded in two pictures that he used in lectures that he held at this time. In the first (Fig. 2), we are reminded of the importance of the mean free path for energy exchanges of the incoming neutron with the nucleons of the target nucleus. If the particles of the target are removed, the incident neutron is accelerated as it enters the energy depression (representing the attractive mean field of the target nucleus), moves across the system, and then comes out again since the original acceleration on entering ensures that the neutron will have sufficient energy to surmount the barrier encountered on leaving. During the short time spent inside the target, the neutron has very little probability of radiating a γ-ray. However, if we restore the individual particles of the target (represented

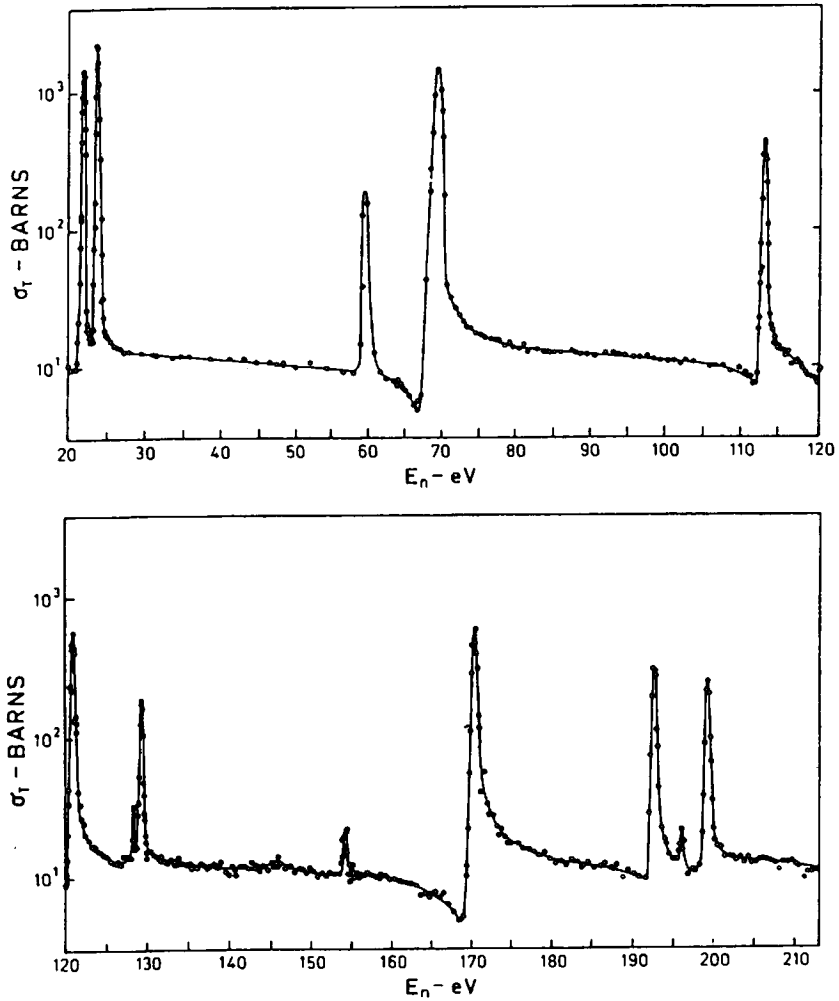

Fig. 1. Experimentally observed resonances in the total cross-section of neutrons scattering on ^{232}Th. The figure is taken from Ref. [1, p. 178].

by billiard balls in Fig. 2), the incoming neutron will have a high probability of colliding with one of these target nucleons (Bohr emphasized the "close packed" nature of nuclear matter; indeed, if we use modern values for the density of nuclear matter, $\rho = 0.17$ nucleon/fm^3, and the range a of the strong interactions $a \sim 1$ fm $\Rightarrow \sigma \sim 2\pi a^2 \sim 6$ fm^2, the classical kinetic theory estimate for the

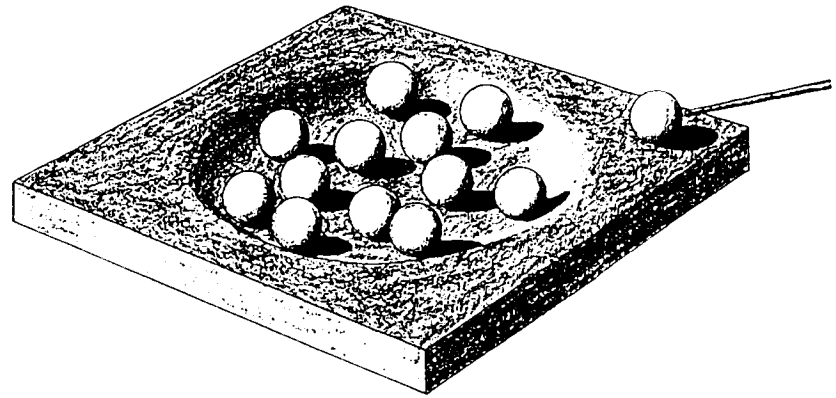

Fig. 2. Figure from Ref. [45]. See discussion in text.

mean free path is $\lambda = (\rho\sigma)^{-1} \sim 1$ fm, which is small compared with the size of a heavy nucleus). Already the first collision implies a sharing of the energy of the incident neutron with the target nucleon so that neither will be able to escape from the nuclear binding field; subsequent collisions of the incident neutron and between the excited nucleons of the target will lead to a complicated state of motion which Bohr called the "compound nucleus" – a state in which the excitation energy is distributed statistically among all the available degrees of freedom of the composite system. Only as the result of a very rare fluctuation will all the excitation energy be again concentrated on a single neutron, which will then be able to leave the nucleus and return to the continuum in an elastic scattering event. The enormous increase in the duration of the reaction process implies a corresponding increase in the probability of gamma-ray emission and therefore in the ratio of the capture to scattering process. Similarly, the long time, τ_{comp} involved in coming back to the original configuration implies a corresponding reduction in the energy scale for resonance structures associated with this process $\Delta E_{res} \sim \hbar/\tau_{comp}$.

The second picture that Bohr employed in discussing these ideas (Fig. 3) was a schematic drawing of the spectrum of the quantum energy levels of a heavy nucleus. It was known experimentally that the lowest excited states in such nuclei had energies of order a few hundred keV above the ground state, and Bohr, in keeping with his view of the nucleus as a strongly interacting many-body system, expected these low-lying states to reflect the normal modes of motion (surface vibrations, compressive modes, and collection rotation) of the nuclear substance. With increasing excitation energy, the number of ways in which the total energy can be divided among these different modes increase exponentially and therefore the level density of the quantum states of the compound nucleus will increase

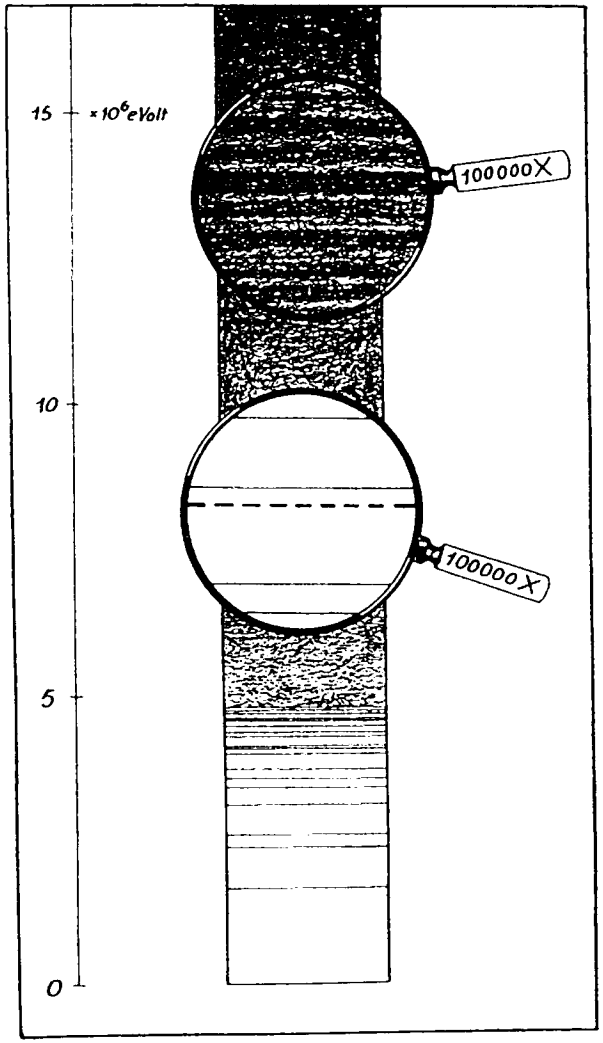

Fig. 3. Figure from Ref. [45]. See discussion in text.

correspondingly. The magnifying glass at about 8 MeV of excitation energy is looking at the region of the spectrum that is studied in low-energy neutron resonance reactions; the dashed line represents the neutron separation energy, and thus the levels above this line appear as neutron resonances, while those below

this line are stable bound states as far as the nuclear interactions are concerned, but can decay to lower bound states by γ-emission. The figure emphasizes the fact that the nuclear levels above and below this level are very similar, and indeed Bohr's concept of the compound nucleus suggests that we should view these different quantal levels in a given energy region as essentially identical in the same sense that almost all classical orbits with a given energy in an ergodic dynamical system are identical since they explore the same regions of phase space with the same probabilities.

The pictures and the language of the last two paragraphs tell us unmistakably that with the concepts of the compound nucleus we are entering a universe in which statistical laws will play a central role. Wigner's introduction of random matrices (1955) represented a major step forward in developing the statistical tools that can be used to express the consequences for quantal spectra of the chaotic dynamics assumed in Bohr's compound nucleus.* The introduction of such a statistical description is usually, in the nuclear physics literature, motivated by asserting that after having studied 100 or 1000 levels in some nucleus, we cannot be expected to attach much significance to the detailed properties of the next single level, and thus we are motivated to accept a description that concerns only average or statistical aspects of the spectrum. I feel that such an approach is profoundly wrong – it is not a blasé relation to the details but exactly the opposite search for the signals that would reveal the impossibility in principle of finding additional quantum numbers hidden in the quantal spectra of nuclei that motivates our study of random matrices (or any other tools that can quantitatively measure the consequences of chaotic dynamics in nuclear spectra).

The basic idea in random matrices is that we shall be attempting to describe a limited energy interval of the spectrum in which the complexity of the underlying dynamics ensures that every eigenstate is a random mixture of all the available degrees of freedom within that energy region. In such a situation, we can expand the Hamiltonian in an arbitrary basis that spans the relevant region of phase space. If there are N basis states in this region, the Hamiltonian becomes an $N \times N$ Hermitian matrix. We shall in addition assume that the matrix is invariant under time reversal (since we are thinking in terms of bound states, but shall also use the results for the very weakly unbound states encountered in the slow neutron resonances), which implies that the basis can be chosen so that the matrix elements of H are real numbers. Taken together, these symmetries imply that we are considering an $N \times N$ real symmetric matrix. We can view the $\frac{1}{2}N(N+1)$ different

* The following discussion of random matrices is necessarily only a very brief introduction to this rich and still actively developing area of quantal physics. The interested reader should consult the Les Houches lectures of O. Bohigas [2] or the classic review article by T.A. Brody et al. [3]. Modern developments in random matrix theory have especially focused on the problems of electronic orbits in simple atoms and transport in mesoscopic systems (see, for example, A.D. Stone et al. [4]).

matrix elements as components of a vector H. The statistical element comes in when we argue that the assumed complexity of the underlying dynamics (identity of almost all classical orbits in phase space) implies that the matrix should be a typical example selected from an ensemble in which the different matrices H are assigned probabilities $P(H)$. The assignment of the probabilities follows from two assumptions:

(1) $P(H)$ should be invariant under orthogonal transformations in the N-dimensional space of the basis functions. This invariance essentially expresses the original assumption that we were expanding H in an arbitrary set of basis functions that span the space and the results of the analysis would be the same if we had chosen almost any other basis set.

(2) The lack of conserved quantities and complexity of the underlying motion of the compound nucleus is exploited once again when we assume that $P(H)$ should be that function which minimizes the *a priori* information $A[P]$ about H as defined in the theory of information

$$A[P] = \int P(H) \ln P(H)\, dH \tag{1.6}$$

The minimum of A must be taken subject to the restrictions imposed by the constraints

$$\int P(H)\, dH = C_0 \tag{1.7}$$

$$\int P(H) \operatorname{tr} H\, dH = C_1 \tag{1.8}$$

$$\int P(H) \operatorname{tr} H^2\, dH = C_2 \tag{1.9}$$

where the condition (1.7) is necessary in order that the probabilities defined by P be normalized, (1.9) and (1.10) define the mean energy and mean level spacing of the part of the spectrum being studied. The conditions (1.7), (1.8) and (1.9) are imposed by introducing Lagrangian multipliers $\{\lambda_i\}$ and minimizing the functional

$$A'[P] = \int P(H) \ln P(H)\, dH - \int (\lambda_0 + \lambda_1 \operatorname{tr} H + \lambda_2 \operatorname{tr} H^2) P(H)\, dH \tag{1.10}$$

which yields the Gaussian orthogonal ensemble

$$P(H) = (C) \exp\left\{ -\sum_{i=1}^{N} \frac{(H_{ii} - a)^2}{2\sigma^2} - \sum_{i<j} \frac{H_{ij}^2}{\sigma^2} \right\} \tag{1.11}$$

where C is proportional to C_0, a to C_1, and σ to C_2. Note that each of the components of H is independently a Gaussian random variable in the ensemble P.

The expression (1.11) characterizes the probabilities of the different matrices H in the ensemble, but we are interested in the eigenvalues and eigenfunctions of the individual matrices. To obtain the distribution of these quantities from that of the H_{ij}, we must diagonalize matrices of the original distribution which is achieved by means of an N-dimensional orthogonal transformation $O_{\alpha i}$; in this manner, each matrix $\{H_{ij}\}$ defines N eigenvalues $\{E_\alpha\}$ and $\frac{1}{2}N(N-1)$ angles $\{\theta_k\}$ in the N-dimensional space of the basis functions. The probability distribution $P(H)$ thus defines a probability distribution $P(\{E_\alpha, \theta_k\})$ in the space of eigenvalues and eigenvectors. To obtain this latter distribution, we note that

$$P(\{E_\alpha \theta_k\}) = C^1 \exp\left\{ -\sum \frac{(E_\alpha - a)^2}{2\sigma^2} \right\} J \tag{1.12}$$

where J is the Jacobian of the transformation that relates $\{H_{ij}\}$ to $\{E_\alpha \theta_k\}$

$$J = \frac{\partial H}{\partial(E, \Theta)} = \det \begin{vmatrix} \frac{\partial H_{11}}{\partial E_1} & \frac{\partial H_{12}}{\partial E_1} & \frac{\partial H_{13}}{\partial E_1} & \cdots & \frac{\partial H_{NN}}{\partial E_1} \\ \frac{\partial H_{11}}{\partial E_2} & \cdots & \cdots & \cdots & \cdots \\ \vdots & & & & \\ \frac{\partial H_{11}}{\partial E_N} & \cdots & & & \\ \vdots & & & & \\ \frac{\partial H_{11}}{\partial \theta_M} & \cdots & & & \frac{\partial H_{NN}}{\partial \theta_M} \end{vmatrix} \tag{1.13}$$

The exponential term on the right-hand side in (1.12) reflects the fact that $\operatorname{tr} H^n$ is invariant under an orthogonal transformation of H and therefore will have the same value in the original and in the diagonalized basis. Since

$$\tilde{O} H O = E = \begin{pmatrix} E_1 & & & \\ & E_2 & & 0 \\ & & \ddots & \\ & 0 & & \\ & & & E_N \end{pmatrix} \tag{1.14}$$

the original matrix elements H_{ij} can be expressed in terms of the eigenvalues and eigenfunctions in the diagonalized basis

$$H_{ij} = \sum_\alpha O_{i\alpha} E_\alpha O_{j\alpha} \tag{1.15}$$

Thus,

$$\frac{\delta H_{ij}}{\delta E_\alpha} = \sum_\alpha O_{i\alpha} O_{j\alpha}$$

$$\frac{\delta H_{ij}}{\delta \theta_\alpha} = \text{linear function of } \{E_\alpha\} \tag{1.16}$$

Inserting (1.16) into (1.13), we find that the first N rows of the determinant in (1.13) are independent of $\{E_\alpha\}$, while the remaining $\frac{1}{2}N(N-1)$ rows have elements, each of which is linear in the eigenvalues $\{E_\alpha\}$. Thus, J is a polynomial of order $\frac{1}{2}N(N-1)$ in the eigenvalues E_α. We also observe that if any two of the eigenvalues are equal, $E_\alpha = E_\beta$, eigenstates are not determined since any linear combination of $|\alpha\rangle$ and $|\beta\rangle$ is also an eigenstate. Thus, J must vanish (the transformation from H_{ij} to $(E_\alpha \theta_k)$ is not defined), i.e., it must contain at least one factor of $|E_\alpha - E_\beta|$. Since

$$\prod_{\alpha<\beta}^{N} |E_\alpha - E_\beta|$$

is already of degree $\frac{1}{2}N(N-1)$ in the eigenvalues, we conclude that

$$J = \prod_{\alpha<\beta}^{N} |E_\alpha - E_\beta| F(\{\theta_k\}) \tag{1.17}$$

The expressions (1.12) and (1.17) provide the starting point for the detailed study of the patterns and correlations in the spectra of the Gaussian orthogonal ensemble. Rather elaborate and elegant mathematical tools have been developed in order to quantitatively evaluate these structures. A proper presentation of this formalism is beyond the scope of the present chapter, but already the form of the results (1.12) and (1.17) provides a simple basis for understanding the main results of this analysis:

1. If E_α and E_β are adjacent eigenvalues in the spectrum, the factor $|E_\alpha - E_\beta|$ in (1.17) can be interpreted as a "repulsion" of near-lying levels, which leads to a low probability for very small spacings. Indeed, if we consider the random matrix for a simple two-level situation, $N = 2$, we get from the above analysis the probability distribution

$$P_W(S) = \frac{\pi}{2} S \exp(-\frac{\pi}{4} S^2) \tag{1.18}$$

$$S \equiv \frac{|E_1 - E_2|}{\langle |E_1 - E_2| \rangle}$$

The distribution (1.18) (the Wigner distribution) differs strikingly from the Poisson distribution

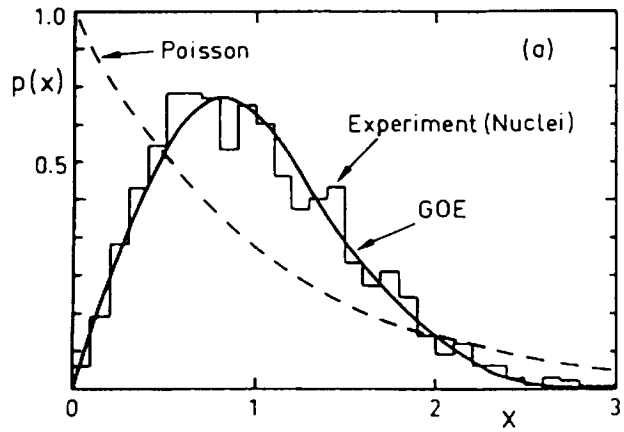

Fig. 4. Probability distribution for energy spacings of nearest neighbor levels in nuclear spectra at excitation energies of order 8 MeV. The quantity, x, measures the observed spacing in units of the average spacing observed in that particular nucleus. Figure from Bohigas [2].

$$P_{poisson}(S) = e^{-S}$$

that would be expected for nearest-neighbors if the eigenvalues $\{E_\alpha\}$ were assumed to be independent random variables distributed with a unit average density. The Wigner distribution reflects the improbability of simultaneously fulfilling the *two* conditions, $H_{11} = H_{22}$ and $H_{12} = 0$ in the original 2×2 random matrix. In fact, the Wigner distribution is a very good approximation to the exact results for the nearest-neighbor distribution obtained from (1.12) and (1.17); in the limit $N \gg 1$, the two are never different by as much as $\delta P = 0.01$. Fig. 4 shows the experimental data on the nearest-neighbor spacing distribution for nuclear levels of the same spin and parity and at an excitation energy of 8–10 MeV. The figure is obtained by combining measurements of resonance energies from many different nuclei assuming that the spacing distribution is a universal function and therefore the only scaling necessary in combining the spacings from different nuclei is that associated with the mean spacing in each nucleus.

2. The Jacobian (1.17) contains factors $|E_\alpha - E_\beta|$ not only for nearest neighbors, but also for all pairs of levels in the spectrum. This fact was especially emphasized by Dyson, who pointed out that the expressions (1.12) and (1.17) can be viewed as the Boltzmann factor appearing in the partition function for a classical gas of N particles with positions $\{E_\alpha\}$ along the one-dimensional E-axis; the particles are held together by a harmonic one-body potential

$$V_1(E_\alpha) = \frac{1}{2\sigma^2}(E_\alpha - a)^2 \tag{1.19}$$

and repel each other with the long range two-body potential

$$V_{\alpha\beta} = -\ln|E_\alpha - E_\beta| \tag{1.20}$$

The long-range nature of the interaction (1.20) implies the very efficient suppression of long wavelength density fluctuations in this one-component plasma. This long-range order in the spectrum is especially apparent in the statistic Δ_3 introduced by Dyson. We consider the function $N(E)$ that counts the number of levels in the spectrum with energy less than E. The statistic Δ_3 measures the deviation of $N(E)$ from a simple linear function of E over an interval of the spectrum where the average level spacing is assumed to be constant

$$\Delta_3(L) \equiv \min_{(A,B)} \frac{1}{L}\int_\alpha^{L+\alpha} dE\,[N(E) - A - BE]^2 \tag{1.21}$$

If the eigenvalues were independent random variables, the resulting *Poisson* distribution describes a random walk for which

$$(\Delta_3(L))_{poisson} = \frac{1}{15}\frac{L}{D} \tag{1.22}$$

where D is the mean level spacing. The long-range repulsion in the random matrix spectrum, in contrast, yields

$$(\Delta_3(L))_{GOE} = \frac{1}{\pi^2}\left\{\ln\frac{L}{D} - 0.0687\right\} \tag{1.23}$$

which, as seen in Fig. 5, is in excellent agreement with the data on resonance energies in nuclei.

3. The random matrix model implies that each of the N eigenfunctions is a random linear combination of the N basis functions subject only to the restriction imposed by the requirement that the different eigenfunctions must be orthogonal. This implies that the probability distribution for the amplitude, $C_i(\alpha)$, for a given basis state $|i\rangle$ in a compound state $|\alpha\rangle$ will be

$$P\,(C_i(\alpha)) = \sqrt{\frac{N}{2\pi}}\exp\left\{-\frac{N}{2}C_i^2(\alpha)\right\} \tag{1.24}$$

in the limit $N \gg 1$. Since in most experiments one measures the square of the probability amplitude, this result is usually written in terms of the probability distribution for $C_i^2(\alpha)$

$$P_{PT}(C_i^2(\alpha)) = \sqrt{\frac{N}{2\pi C_i^2(\alpha)}}\exp\left\{-\frac{N}{2}C_i^2(\alpha)\right\} \tag{1.25}$$

which is called the Porter–Thomas distribution. One should note the very large fluctuations implied by the Porter–Thomas distribution:

$$\langle C_i^2(\alpha)\rangle = \frac{1}{N}$$

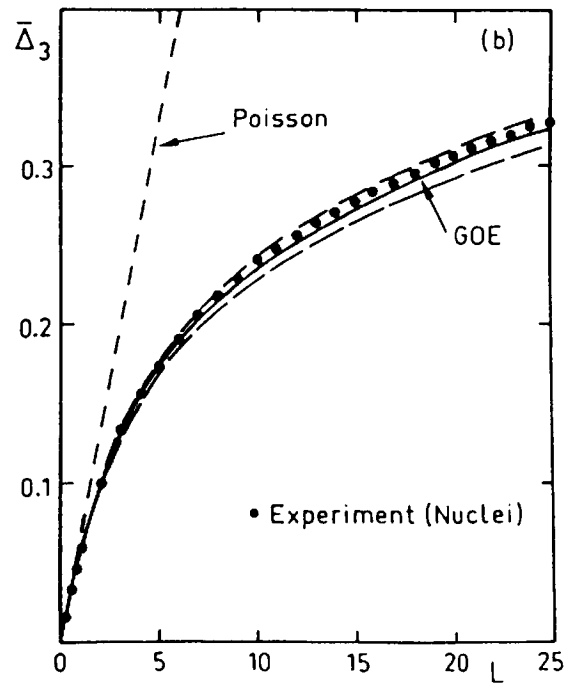

Fig. 5. Observed values for the statistic Δ_3 measured in nuclear spectra at excitation energies of order 8 MeV. Figure from Bohigas [2].

$$\langle (C_i^2(\alpha))^2\rangle - \langle C_i^2(\alpha)\rangle^2 = \frac{2}{N}$$

The reduced neutron width of a neutron resonance measures the probability in the resonance state of the unique basis component, in which the neutron is in the scattering state in the continuum and all the other nucleons are in the ground-state configuration of the target nucleus, and thus the fluctuations in these neutron widths are expected to be described by the distribution (1.25); the comparison with experimental data is shown in Fig. 6.

4. The above discussion of experimental data concerning the fluctuations in widths and spacings of resonance states establishes a very convincing agreement with the predictions of the random-matrix theory for these quantities. However, it must be remembered that this data, in all the cases considered, covers a very narrow energy interval, ΔE, of the spectrum (typically $\Delta E \lesssim 1$ keV for the neutron resonance data) and this implies that the information on nuclear dynamics concerns effects that are averaged over a rather long time interval $\tau \sim \frac{\hbar}{\Delta E} \gtrsim$

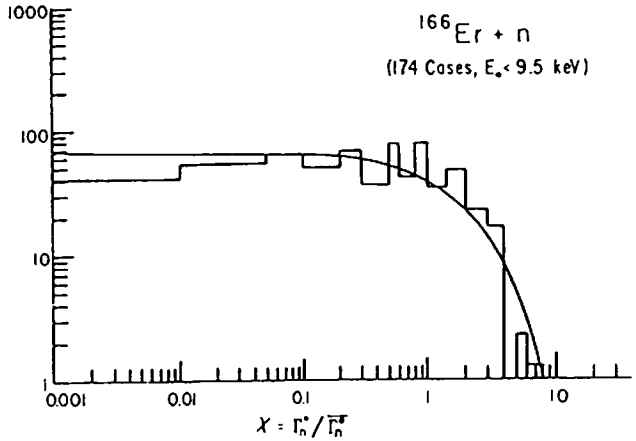

Fig. 6. Probability distribution for the reduced neutron width, $\Gamma_n^{(0)}$, measured for resonances observed in neutron scattering on ^{166}Er. The solid line corresponds to the Porter–Thomas distribution (Eq. 1.25). The data is from Liou et al. [46].

10^{-18} s. The assumptions made in formulating random-matrix theory postulate the existence of a complete mixing of all the available degrees of freedom and thus in this model there is no characteristic time for formation of the chaotic motion. It thus seems probable that the impressive agreement with the theory may reflect the fact that we have not been able to study the processes that occur on a shorter time scale. Indeed, as we shall see in later chapters, typical periods for single-particle motions are $\tau_{sp} \sim \frac{R}{v_F} \sim 10^{-22}$ s, and for nuclear vibrations $\tau_{vib} \sim 10^{-21} - 10^{-22}$ s. It does not seem likely that the methods employed in obtaining the data in Figs. 4–6 can be extended to study temporal processes on such scales, but the development of powerful new spectroscopic tools for the study of yrast spectroscopy holds promise of providing data that may explore the limits of the random-matrix model and shed light on the time scales involved in the establishment of chaotic dynamics in nuclei (see, for example, J.D. Garrett et al. [5]).

2. Independent particle motion

The picture of nuclear structure associated with the compound nucleus provided an impressively successful basis for interpreting the growing body of information about nuclear properties for more than a decade, but then in the late 1940's this picture was profoundly challenged by the evidence of shell structure in

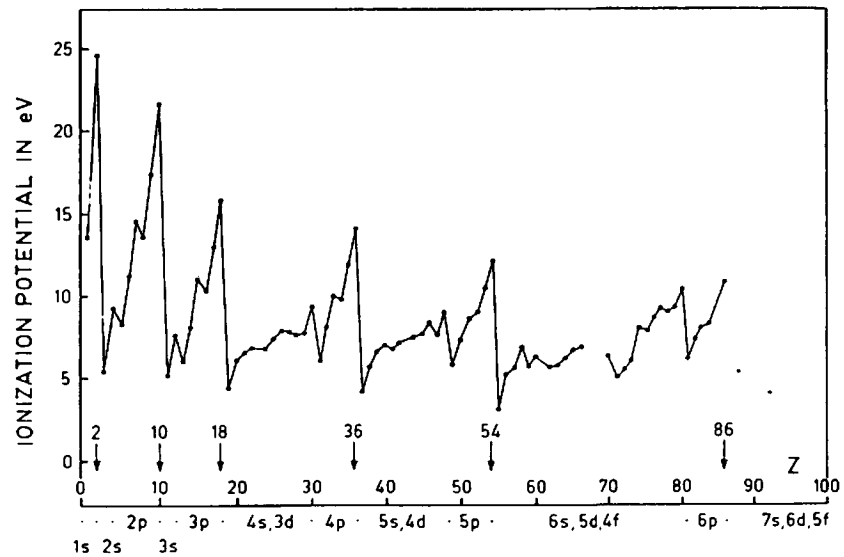

Fig. 7. Atomic ionization energy as a function of the atomic number, Z. The dots under the abscissa indicate electronic ground state configurations comprised of completed shells. The figure is from Ref. [1, p. 191].

the binding energies of nuclei [6]. The framework for presenting and interpreting this evidence could be directly appropriated from the experience in atomic physics, where the special stability and chemical inertness of the noble gas atoms ($_2$He, $_{10}$Ne, $_{18}$Ar, $_{36}$Kr, $_{54}$Xe, and $_{86}$Rn) are immediately explained by the quantal energy spectrum of the individual electrons moving in the mean field potential of the atom; see, for example, Fig. 7 which shows the variation of the atomic ionization potential that directly measures the binding energy of the last filled electronic orbit. In a similar manner, the binding energies of nuclei reveal the existence of discontinuities in the separation energies of neutrons or protons associated with the "magic numbers"

$$N \text{ or } Z = 2,\ 8,\ 20,\ 50,\ 82 \text{ and } 126 \tag{2.1}$$

(see the examples shown in Figs. 8 and 9). These discontinuities reflect a "bunchiness" in the spectrum of the one-particle motion in the nuclear potential; when all the orbits in one bunch are filled, the system has a special stability. A nucleus with one more particle must involve a configuration in which one of the orbits in the next higher "shell" is occupied; this will be a less strongly bound configuration and the last particle can be removed with a relatively smaller separation energy.

Within less than a year after the evidence for "magic numbers" had been pre-

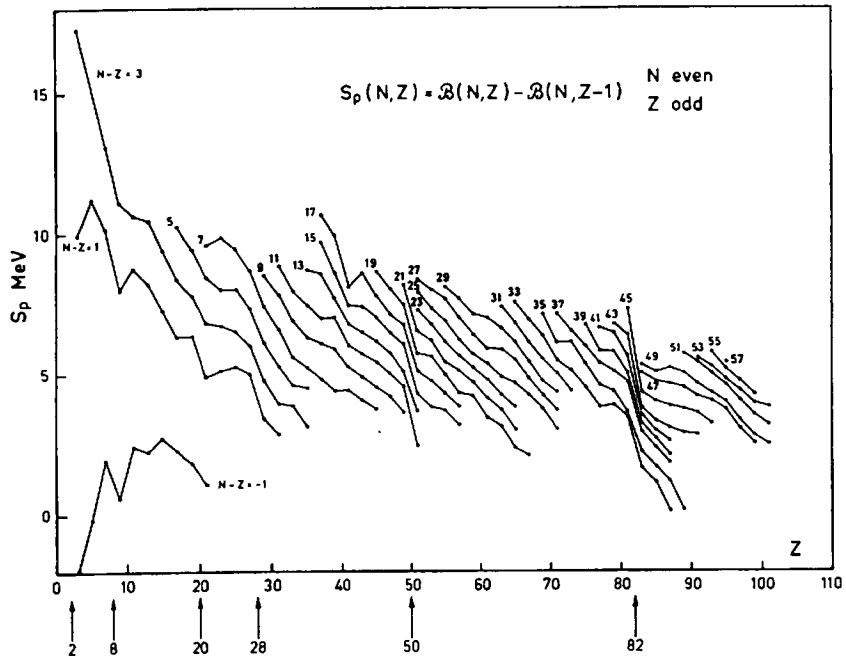

Fig. 8. Proton separation energies as function of proton number, Z. Points connected by straight lines correspond to constant neutron excess, $N - Z$. The figure is from Ref. [1, p. 194].

sented, the appropriate nuclear potentials that explained the shell structure were found by Mayer [7] and independently by Haxel, Jensen and Suess [8]; these potentials involve, besides a central, attractive potential, a relatively strong spin–orbit interaction that gives a greater binding to particles with parallel spin and orbital angular momentum as compared with orbits with anti-parallel spin and orbit. An example of the spectrum resulting from such a potential is shown in Fig. 10, where it is possible to directly see the bunchiness responsible for the "magic numbers" summarized in Eq. (2.1). Extensive studies of the nuclei with a single particle added to or missing from a closed shell have provided confirmation in exquisite detail of the spectrum of single-particle levels implied by Fig. 10 (compare, for example, the calculated spectrum of Fig. 10 with the observed spectra of ^{207}Pb and ^{209}Pb shown in Fig. 11); this confirmation extends not only to the angular momentum and parities of the individual orbits, but also to moments, transition matrix elements, and selection rules for transitions between these configurations. In making this comparison with experimental data, it is important to recognize that a single nucleon propagating through the nuclear medium creates a cloud

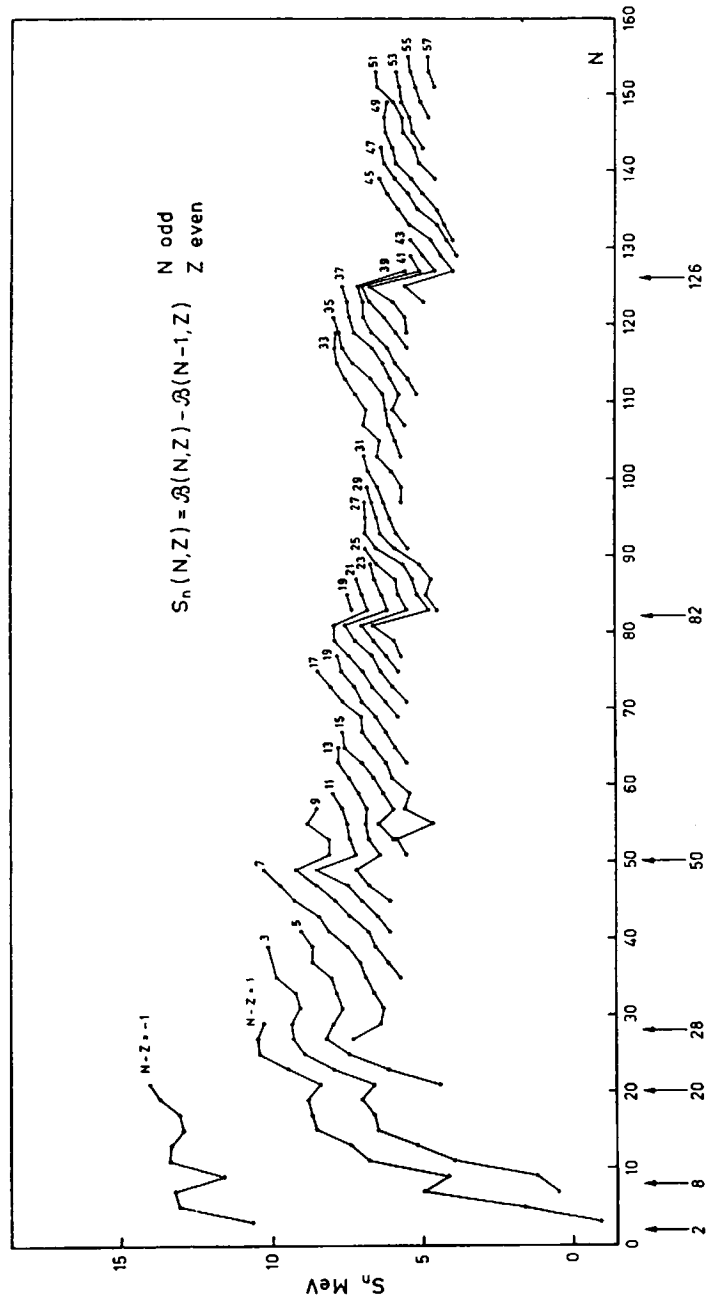

Fig. 9. Neutron separation energies as function of neutron number, N. Points connected by straight lines correspond to constant neutron excess, $N - Z$. The figure is from Ref. [1, p. 193].

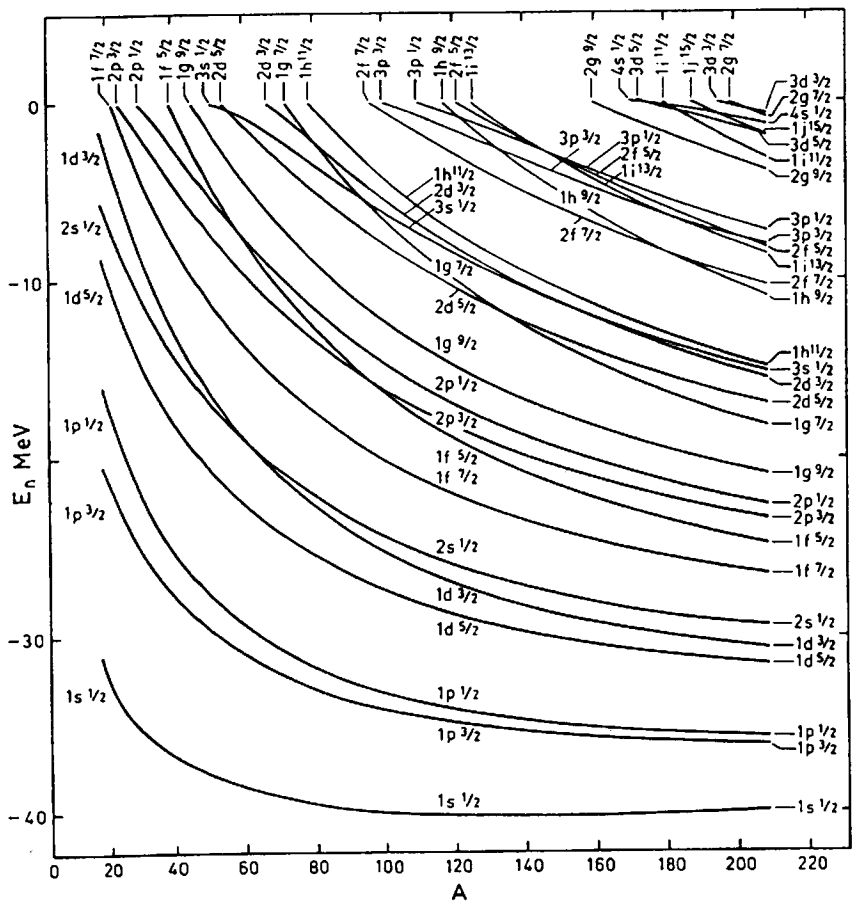

Fig. 10. Calculated single-particle energies for Woods–Saxon potential with spin–orbit force. The radius of the potential is assumed to depend on mass number, A, as $R = r_0 A^{1/3}$, $r_0 = 1.27$ fm. The figure is from Ref. [1, p. 389].

of excitations that follow the particle around and contribute significantly to the various matrix elements; thus it is the "dressed" particles, or quasi-particles, that move in the orbits of Fig. 10 and whose matrix elements describe the observed transitions.

Although the detailed examination of these polarization effects is a fascinating and important element in a systematic exposition of nuclear structure, it is outside the scope of the present chapters and therefore I shall now attempt to discuss the more general matters of principle raised by the apparent discrepancy between

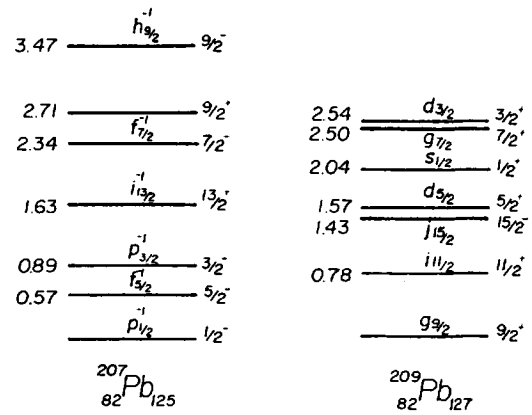

Fig. 11. Observed low energy spectra for ^{207}Pb and ^{209}Pb. The independent particle description of these two nuclei implies that the lowest quantum states should correspond to configurations of a single neutron (for ^{209}Pb) or a single neutron hole (for ^{207}Pb) in addition to the closed shell configuration of ^{208}Pb. The data for this figure is taken from the compilation by R.B. Firestone [47].

the independent particle picture implied by the data referred to above and the compound nucleus discussed in the previous chapter. There are three separate issues that must be addressed:

1. What is the mean free path for energy exchange when a nucleon moves through the nucleus?

2. How can the evidence for chaotic structures (absence of conserved quantum numbers) be reconciled with the evidence for shell structure which builds on the existence of conserved single particle quantum numbers for each of the occupied orbits?

3. How can the independent particle motion survive in the presence of the very strong, short-range, and complicated forces that act between each pair of nucleons?

We address each of these questions in turn:

1. The mean free path for a nucleon moving through a target nucleus can be directly measured in scattering experiments, as indicated in Fig. 12. An incident wave will be accelerated on entering the target, because of the nuclear attraction, and will then have a somewhat shorter wave length while inside the nucleus:

$$K_{in} = \sqrt{K_{out}^2 + \frac{2MV_o}{\hbar^2}} \tag{2.2}$$

where V_o is the magnitude of the attractive potential. Thus, the transmitted wave will have a phase shift with respect to the incident wave; and since the magnitude

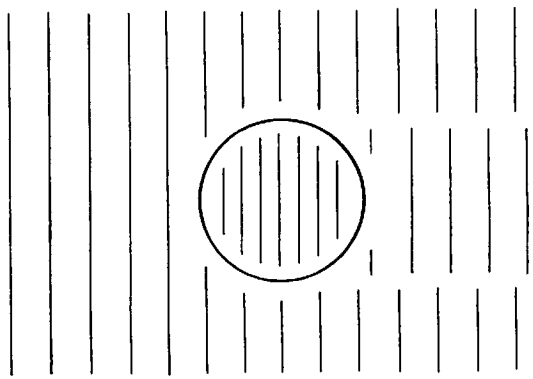

Fig. 12. Schematic picture of wave fronts for a plane wave of neutrons incident on a nucleus. The incident neutrons arrive from the left of the target nucleus and the interference of the transmitted and incident wave is indicated on the right.

of this phase shift will depend on the bombarding energy

$$\text{phase shift} \sim (K_{in} - K_{out}) \times (\text{path in nucleus}) \tag{2.3}$$

the interference between the transmitted and incident wave will give rise to oscillations in the cross section as a function of energy. The phase shift is a decreasing function of energy and an increasing function of the nuclear size (which determines the path length), and thus the maxima and minima in the cross sections shift to lower bombarding energies with increasing nuclear size (compare the experimental cross sections in Fig. 13). The effect of a finite mean free path, λ, can be included by adding an imaginary term to the wave number in (2.2):

$$K_{in} = \sqrt{K_{out}^2 + \frac{2MV_o}{\hbar^2}} + \frac{i}{2\lambda} \tag{2.4}$$

which will imply an attenuation of the transmitted wave as it passes through the nucleus. Note that the factor 2 multiplying λ reflects the fact that the mean free path is defined in terms of the attenuation in the probability of the transmitted wave (attenuation of the flux). If λ were small compared with the nuclear radius, the transmitted wave would have negligible intensity and the total cross sections would be a universal monotonically decreasing function of the bombarding energy (black nucleus). The observed cross sections (Fig. 12) exhibit marked oscillations that define the "optical potential" for low energies ($E_n \lesssim 2$ MeV)

$$V_o = 50 \text{ MeV}$$
$$\lambda = 30 \text{ fm} \tag{2.5}$$

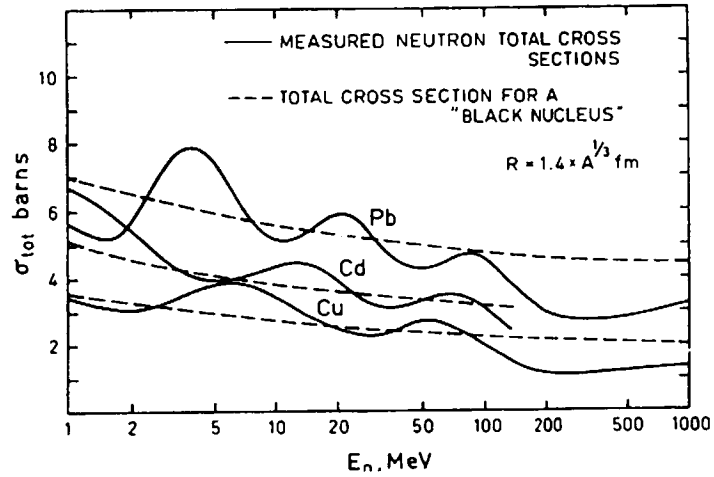

Fig. 13. Observed total cross-sections as function of energy for neutron scattering on Cu, Cd, and Pb. The figure is taken from Ref. [1, p. 165].

Thus, the mean free path is long compared to the nuclear size for a nucleon with energy close to the Fermi energy, in agreement with the evidence for shell structure in the nuclear spectra, but in striking disagreement with Bohr's assumption which had provided the starting point for the formulation of the concepts associated with the compound nucleus.

2. The apparent conflict sketched in the last sentence of the previous paragraph can be resolved by examining the different time scales associated with experimental studies that are separately interpreted in terms of chaotic and independent particle structures in the nuclear dynamics:

(a) traversal time, τ_o, for a nucleon in the nucleus:

$$\tau_o = \frac{2R_o}{v_F} \sim 10^{-22} \text{ s}. \tag{2.6}$$

(b) collision time:

$$t_{col} = \frac{\lambda}{v_F} \sim 3 \times 10^{-22} \tag{2.7}$$

where λ is the mean free path for a nucleon with energy within a few MeV of E_F;

(c) single particle residence time, t_{in}, for a reaction involving an incident slow neutron ($E_n \sim 10$ eV):

$$t_{in} = \frac{\tau_o}{\mathrm{T}} \sim 10^{-19} \text{ s} \tag{2.8}$$

where T is the transmission coefficient Eq. (1.3).

The condition for the occurrence of shell structure and independent particle motion is

$$\tau_o < t_{col} \tag{2.9}$$

which is, of course, the same as $\lambda > R$, while the individual resonances will exhibit the chaotic features of the compound nucleus if

$$t_{in} > t_{col} \tag{2.10}$$

The condition (2.10) is well satisfied despite the long mean free path because of the very small value of the transmission coefficient, T, resulting from the extreme mismatch between the neutron energy inside and outside the nucleus. Only when the coherent effects of $\sim 10^4$ or more resonances are observed do the experiments achieve a time resolution that is sufficient to reveal the underlying periodicities associated with single-particle motion.

The conclusion of this brief exploration of the boundaries between order and chaos in the nuclear dynamics is that the extreme cases of single-particle motion on time scales of order τ_o and chaotic behavior on scales of order t_{in} have been characterized in considerable detail, but the cross-over regime somewhere in between remains as an important topic of current investigation.

3. The essence of shell structure and its interpretation in terms of independent particle motion is the fact that the orbits of the individual nucleons are delocalized and their eigenvalues therefore reflect the shape and radial dependence of the potential over the whole nuclear volume. After the discovery of shell structures in nuclei, it became a major challenge to many-body theory to understand how this delocalized structure can be reconciled with the very strong and short-ranged forces that are observed to act when individual nucleons are scattered off each other in laboratory experiments. A detailed discussion of this question would involve consideration of the various rather complicated features of the observed nuclear forces, and is beyond the scope of the present chapters. We shall instead discuss the essence of the issues involved by considering the more schematized problem of the structure of the ground states for an infinite system of fermions interacting with the central spin-independent short-ranged forces illustrated in Fig. 14. This will permit us to address the basic issues without too much complication.

The important features of the nuclear interaction as sketched are the large values of the potential energies involved – attractions of order 100 MeV and repulsion at shorter distance of order 1000 MeV. How can delocalized independent particle motion survive in the presence of these forces? The text books and literature agree with near total unanimity that the answer to this question is provided by the effects of the Pauli principle and the Fermi distribution. The argument is that, when two particles within the Fermi distribution interact, they cannot be scattered into states that are near-lying in energy and momentum because such final states

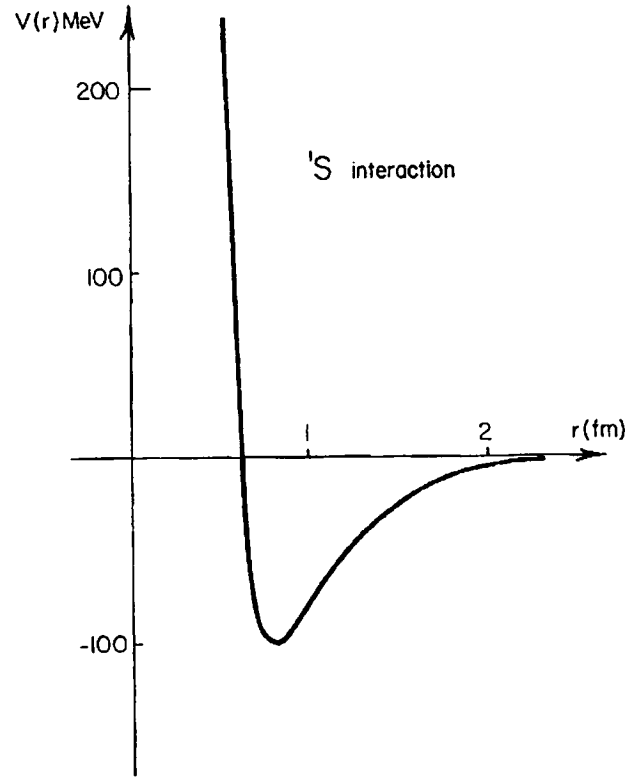

Fig. 14. Observed two-body interaction for nucleons with $S = L = 0$. Using this potential to characterize the numbers appearing in the quantality parameter, we obtain $a = 0.9$ fm, and $V_o = 100$ MeV.

are already occupied. Thus, the perturbation of the Fermi distribution produced by the interactions involves minimal energy exchanges that are of order the Fermi energy, $E_F \sim 40$ MeV in the nuclear medium. This effect of the Pauli principle gives to the independent particle description a "rigidity" which can be more quantitatively exhibited in the apparent rate of convergence of an appropriately rearranged perturbation expansion starting from the non-interacting Fermi gas.

Despite the wide consensus supporting the above explanation and its distinguished pedigree, it is my belief that it is seriously misleading since a delocalized structure and a long mean free path would be just as prominent if nucleons were bosons interacting with the same forces, and thus a more nuanced understanding of the issues involved is necessary if we are to correctly understand the basic fea-

tures of nuclear structure.* Regarding this matter, it is useful to remember that for a many-body system of the type defined above, we know of only two basic designs for the ground state:

(1) For a system described by classical mechanics and short-range forces as in Fig. 14, the lowest energy state is obtained by finding for each particle the equilibrium position that minimizes its potential energy with respect to all its neighbors. Such static, localized structures provide the basic design for the ground states of molecules and crystals.

(2) In quantum mechanics, the zero-point kinetic energy, $\sim \hbar^2/Ma^2$, involved in the localization of a particle within a volume of radius a implies that in the lowest energy state, the particles may be delocalized because the potential energy gain of the classical configuration is overwhelmed by the quantal kinetic energy. Such delocalized quantal fluids provide the basis for discussing the state of electrons in atoms, and metals, of the He atoms in the ground state of the helium liquids (both fermionic ^{3}He, and bosonic ^{4}He), and the state of nucleons in atomic nuclei.

The relative magnitude of the quantal kinetic energy of the localized state compared with the potential energy can be qualitatively characterized by the "quantality" parameter†

$$\Lambda = \frac{\hbar^2}{Ma^2} \cdot \frac{1}{V_o} \tag{2.11}$$

where M is the mass of the individual particles, while V_o and a (see Fig. 14) measure the strength of the attraction and the range corresponding to the minimum of the potential, respectively. When Λ is small, quantal effects are small and the lowest state will have a crystalline structure, while for sufficiently large Λ, the system will remain a quantum fluid even in its ground state. It is crucial for the arguments that follow that Λ does not depend explicitly on the statistics (Bose or Fermi) of the quantal system being considered.

You might, at first, think that there should be a large difference between the value of Λ that defines the limit of the frozen state of Fermi and Bose systems, and in this way the significance of the Pauli principle is upheld. However, this difference is not large as can be understood from the fact that in the frozen state the particles are by definition localized and thus the exchange integrals, that distinguish Fermi and Bose systems, are relatively small; for example, it has been estimated by L.H. Nosanov [9] that, for interactions such as those that act between He atoms, the critical value of Λ characterizing the transition from fluid to crystal differs by only about 25% depending on whether the statistics are those of fermions or bosons.

* I am aware that there is a lively and active many-body community that is well aware of most, if not all, of the arguments that I shall be presenting in the rest of this chapter. However, the failure of their message to have had any noticeable impact on the thinking of the rest of the nuclear physics community provides me with the motivation for trying to present the arguments here.

† A parameter related to Λ was employed in 1938 by De Boer in order to interpret the relative magnitude of quantal effects in the weakly bound crystals formed by noble gas atoms. Again, in 1948, De Boer used this parameter to correctly predict the critical temperature and pressure of ^{3}He more than a year before it was experimentally measured [10,11].

Table 1

The mass M is in units of the proton mass ($M_p = 1.67 \times 10^{-24}$ gm = 0.938 GeV/c^2); the parameters V_o and a are the depth of the potential minimum and the separation at which it occurs, while the numbers in parentheses give the power of 10 multiplying the listed value. The nuclear force (from Fig. 14) corresponds approximately with the ^{1}S central force in $T = 1$ states for the Argonne v_{14} potential [13] while the parameters for the atomic systems are the Lennard-Jones potentials given by J. De Boer [12]

Constituents	M	a (cm)	V_o (eV)	Λ	$T = 0$ grand design
^{3}He	3	2.9 (−8)	8.6 (−4)	0.19	liquid
^{4}He	4	2.9 (−8)	8.6 (−4)	0.14	liquid
H_2	2	3.3 (−8)	32 (−4)	0.06	solid
^{20}Ne	20	3.1 (−8)	31 (−4)	0.007	solid
nucleons	1	9 (−14)	100 (+6)	0.5	liquid

The values of the force parameters and the resulting quantality parameters for several condensed matter systems and for nuclear matter are collected in Table 1. It is seen that the transition between quantum liquid and crystalline solid occurs in the region $\Lambda \sim 0.1$ (between He and H_2) and that nuclear matter is safely, by almost a factor of 5, on the side of the quantum liquid structure. It is important to emphasize that if it is accepted that the nuclear forces are too weak to localize the nucleons in a crystalline structure, then there is no alternative (that we know of) to a ground state with delocalized structure and elementary excitations with long mean free path (essentially infinite for excitations close enough to the ground state), and that these features will occur independently of the statistics (bosonic or fermionic) of the constituents. In order to establish the manner in which these features follow from the nature of quantum fluids, it will be necessary for me to briefly review some of the standard results of Fermi and Bose liquid theory.

2.1. Fermi liquids

The basic idea of Fermi liquid theory was given by Landau [14] while more detailed exposition of these ideas are given by Nozieres [15] and Anderson [16] They state that the ground state and low-lying excitations of an interacting Fermi

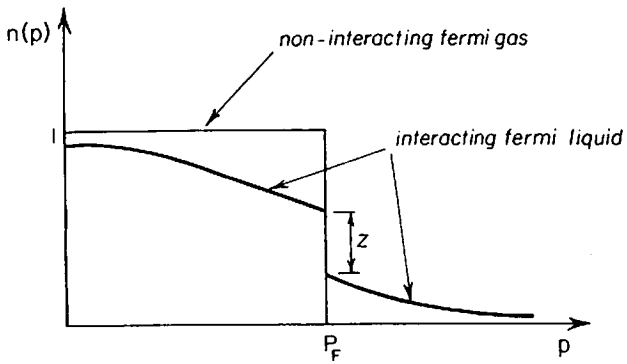

Fig. 15. Momentum distribution for the ground state of an infinite Fermi liquid. See discussion in text.

system can be put into a one-to-one correspondence with the quantum states of the non-interacting system if the interactions are not too strong. For the non-interacting infinite system, the states are labeled by the wave number k, and all states with $|k| \leq k_F$ are filled (the Fermi distribution) and those with $k > k_F$ are empty in the ground state. In the interacting system, the ground state will be described by a linear combination of different anti-symmetrized configurations involving various numbers of particles that have been "scattered" out of the Fermi distribution into states with $|k| > k_F$ (see Fig. 15). It is a striking feature of the interacting Fermi system that to all orders in perturbation theory, the discontinuity of the occupation numbers at the Fermi surface survives [17], although the magnitude of the discontinuity will be decreased below the value $Z = 1$ that characterizes the non-interacting system.

Excited states of the non-interacting system are created by adding one or more particles in states with $|k|$ above k_F or removing particles from states with $|k|$ less than k_F. In the interacting system, adding a particle with $|k|$ slightly greater than k_F will give rise to a spectrum of excitations extending over all energies, but as long as the system is in the Fermi liquid phase, there will be a concentration of strength in the neighborhood of the energy (Fig. 16)

$$E_k = E_F + \frac{\hbar|k. - k_F|k_F}{m^*} \tag{2.12}$$

where m^* is an effective mass that depends on the interactions. This "strength function" of the quasi-particle has an integrated probability equal to Z, the discontinuity parameter, and an energy width, Γ, that goes to zero as $(k - k_F)^2$. Removing a particle with $|k|$ slightly less than k_F produces an excitation in the interacting system with the same properties as those of the above quasi-particle.

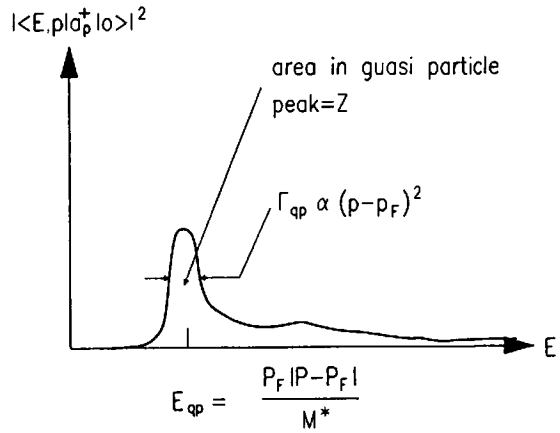

Fig. 16. Schematic figure illustrating the energy spectrum of the states populated when a single fermion in a plane wave state is added to the ground state of a fermi-liquid. See discussion in text.

The fact that these quasi-particles have a decay width reflects the fact that the "bare" particle state is damped by interactions that can mix this state with other many-particle states having the same k and similar energy; the fact that the width goes to zero as $k \to k_F$ reflects the paucity of such states in the low-energy spectrum and ensures that, sufficiently close to the ground state, the width of the quasi-particle will become very small compared with the excitation energy (2.12) and thus ensures that the low-energy spectrum can be described in terms of these quasi-particles and their effective interactions.

Considerable current effort is being directed toward the question of evaluating the correlations in nuclear matter produced by the best available nuclear interactions. Several different approaches are being used (see the review by V.R. Pandiharipande [18]) and it appears that a consensus is emerging for a value of about $Z \approx 0.7$ for nuclear matter. This value can be compared with $Z \approx 0.4$ for the ^{3}He liquid, which reflects the much smaller value of Λ (stronger interactions) for the latter system.

The main conclusion of this brief survey of Fermi liquid theory is that as long as the system is in the Fermi liquid phase, the low energy spectrum will be described by quasi-particle excitations labeled by the quantum numbers of the non-interacting system. Since the validity of these quantum numbers hinges on defining the phase of the nuclear matter, it seems uncertain whether this question can be answered by any rearrangement of perturbation theory. Rather, a theoretical examination of the stability of the Fermi liquid phase must involve a comparison of the calculated energy of this phase with that calculated for some alternative phase. In

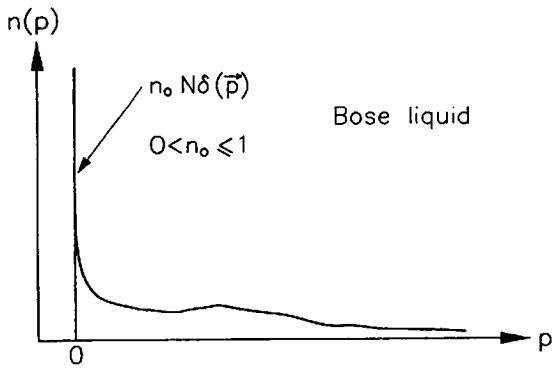

Fig. 17. Momentum distribution for the ground state state of an infinite Bose liquid. For a non-interacting system of bosons in its ground state, all the particles occupy the lowest available single particle state. In the presence of interactions which are not so strong as to cause the system to crystallize, a fraction, n_0, of the particles will still condense into the single lowest particle state, $p = 0$.

fact, of course, the rather large value of Λ implied by the nuclear forces provides very strong support for the belief that the system is in the Fermi liquid phase.

2.2. *Bose liquids*

An important part of the present discussion is the assertion that even if nucleons were bosons interacting with the same forces, the delocalized structure and long mean free path of excitations would survive and provide the "grand design" for the nuclear system. Thus, we must in this section review some of the basic properties of Bose liquids. It is useful, as for Fermi liquids, to begin with the non-interacting system in its ground state and low-lying excitations and then discuss what happens to these quantum states when the interactions are turned on. As is well known, a non-interacting Bose gas in its ground state is described by a wave function in which all the particles occupy the same, $k = 0$, one-particle state (Fig. 17). In the presence of interactions, the particles will develop correlations with respect to each other, and this is described by a wave function which is a linear combination of symmetrized configurations in which various numbers of particles have been scattered into one-particle states with $k \neq 0$. It is a crucial feature of the Bose systems that as long as the interactions are not too strong (i.e. Λ too small), the single one-particle state with $k = 0$ continues to be occupied by a finite fraction, n_o, of all the particles, although $n_o < 1$ in the interacting system just as $Z < 1$ in the interacting Fermi liquids. The low-lying excitations of the non-interacting Bose system are obtained by exciting one or more particles from the $k = 0$ condensate into $k \neq 0$ states. In the presence of interactions, a one-particle excited

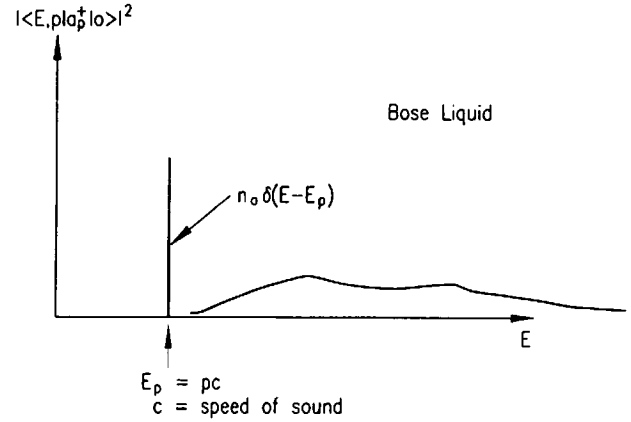

Fig. 18. Schematic figure illustrating the energy spectrum of the states populated when a single boson in a plane wave state is added to the ground state of a Bose liquid.

state, k, becomes "dressed" with a cloud of excitations of the medium to become a longitudinal density wave (phonon) with wave number k. This dressing of the particle implies partly that the probability for exciting the phonon is now proportional to the condensate fraction, n_o, and partly that the energy of the state with momentum k is shifted from the value $\hbar^2k^2/2m$ to the value [19,20] (Fig. 18)

$$E_k = kc \tag{2.13}$$

where c is the speed of sound, which can be obtained from the bulk compressibility of the interacting system. Feynman [21] has presented physical pictures which apparently demonstrate that these phonon excitations are the only excitations permitted by the Bose symmetry at sufficiently low energy and thus their rate of decay is even slower than that of the quasi-particles considered in connection with the low-energy excitations of the Fermi liquids.

The above discussion provides us with the necessary tools for discussing a thought experiment of the type illustrated in Fig. 12, in which the incident particle is a boson being scattered off a droplet of interacting boson matter in its ground state. The incident low-energy particle, on entering the droplet, will be converted into an acoustic wave that will travel unattenuated until it reaches the other side, where it will be re-converted into a particle wave that will then interfere with the incident wave just as in the nuclear scattering experiment. Thus, the conclusion of the experiment will be the confirmation of the long mean free path of a boson moving through bosonic matter in its ground state. The only way in which these features could be lost would be if the interactions were so strong (i.e. Λ so small)

that the interacting system exists in the localized phase (crystalline) in its ground state.

Finally, it should be emphasized that the value of Λ that defines the phase boundary between localized and delocalized phases will not be exactly the same for bosonic and fermionic systems. However, the difference is expected to be rather small because, when the system crystallizes, the localization of the particles implies that the exchange integrals of the interaction are small. Indeed, a calculation of the ground state of ^{3}He assumed to be bosonic or fermionic, with the same (realistic) interactions and the same density as observed in the fermionic ground states, yields values of the condensate fraction n_o and the Fermi surface discontinuity Z that are equal to within the accuracy of the calculations [22].

3. Shell structure

Shell structure is a pervasive theme in the interpretation of finite fermionic many-body systems that fall under the Grand Design of independent particle motion (atoms, clusters of metallic atoms, and atomic nuclei). In all these systems, the level density of single-particle orbits exhibits significant oscillations, and this "bunchiness", called "shell structure", provides the organizing principle for the analysis of the associated many-body system. Configurations involving only closed shells have exceptional stability, low reactivity and, of necessity, some element of symmetry. Configurations with a number of particles outside closed shells exhibit, besides lower stability, a collection of related features referred to as hybridization of orbits, the Jahn–Teller effect, deformation, etc. These aspects of shell structure are well known and are extensively treated in standard texts as resulting from a proper choice of the mean field potential, solution of the one-body Schrödinger equation, and use of the resulting wave function to calculate matrix elements, collective correlations, etc. In the present chapter, we shall be concerned with the more general questions raised by the very existence of this shell structure:*

- Why is there bunchiness in the single-particle spectrum?
- What is its fundamental order of magnitude and how will it scale with particle numbers as $A \to \infty$?
- What features of the mean field are relevant?
- What are the quantum numbers of the orbits that belong together in a single bunch?

* The concepts for addressing these questions were developed by R. Balian and C. Bloch [23], and with a somewhat different emphasis in work by M.C. Gutzwiller [24]. The presentation in the present chapter is based on Ref. [25, p. 578].

The occurrence of shell structure is directly related to geometric symmetries of the mean field potential and in particular symmetries that make possible a separation of variables in the three-dimensional motion of the individual particles. I shall illustrate the ideas involved by considering motion in a spherically symmetric potential, but as we shall see in a later chapter, the analysis can also be fruitfully applied to problems involving non-spherical potentials. Also, in this introduction to the concepts we shall ignore the spin orbit force. With these simplifications, the single-particle eigenvalues, ϵ, depend on two integer quantum numbers: n, the number of nodes in the radial wave functions, and, l, the magnitude of the orbital angular momentum (equal to the number of nodes in the angular dependence of the wave function). Quite generally, $\epsilon(n, l)$ is a function of the quantum numbers that increases monotonically with increasing values for either of the two quantum numbers. This structure in $\epsilon(n, l)$ opens the possibility that approximate degeneracies can occur in the spectrum by a compensation associated with an increase in one of the quantum numbers and at the same time an appropriate decrease in the other quantum number. We can develop this idea more systematically by considering the limit of large quantum numbers, where we can consider $\epsilon(n, l)$ as a smooth function of its variables (asymptotic expansion) and expand around some point (n_o, l_o):

$$\epsilon(n, l) = \epsilon(n_o l_o) + (n - n_o)\left(\frac{\partial \epsilon}{\partial n}\right)_o + (l - l_o)\left(\frac{\partial \epsilon}{\partial l}\right)_o + \frac{1}{2}(n - n_o)^2\left(\frac{\partial^2 \epsilon}{\partial n^2}\right)_o + \cdots \tag{3.1}$$

Since n and l must take on integer values, the possibility of compensation between changes in n and l (at least to first order) is restricted by the condition

$$\left(\frac{\partial \epsilon}{\partial n}\right)_o : \left(\frac{\partial \epsilon}{\partial l}\right)_o = a : b \tag{3.2}$$

where a and b are (small) integers. When condition (3.2) is satisfied, there will occur in the spectrum a set of states with (approximately) degenerate energy

$$\epsilon(n, l) \approx \epsilon(n - \nu b,\ l + \nu a) \quad \nu = \pm 1, \pm 2, \ldots \tag{3.3}$$

Condition (3.2) can be immediately interpreted in terms of the classical mechanics of a particle moving in the assumed potential, since quite generally (see, e.g., H. Goldstein [26], pp. 288 ff)

$$\frac{\partial(\text{energy})}{\partial(\text{action})} = \text{frequency of classical orbit} \tag{3.4}$$

Thus, condition (3.2) implies that the classical motion in the neighborhood of (n_o, l_o) corresponds to three-dimensional periodic orbits. (Note that the separa-

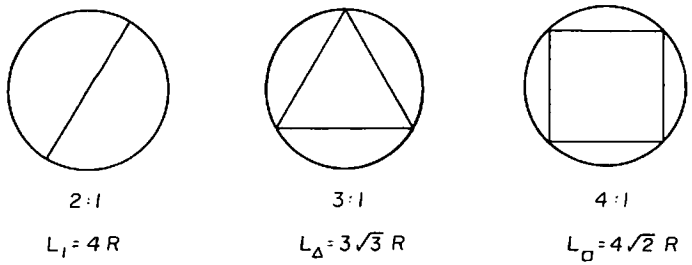

Fig. 19. Simple classical orbits for single particle in constant potential with sharp spherical boundary.

bility of the motion in all three dimensions implies that the orbit is periodic in each of the three coordinates separately, but the three-dimensional motion will in general be multiply periodic with irrational ratios of frequency, i.e., the orbit will resemble a Lissajous figure; conditions (3.2) and (3.3) imply strictly periodic motion, with the orbit closing on itself after a oscillations in the radial direction and b oscillations in the angular motion.) The bunchiness of the quantal spectrum is a reflection of the occurrence of degenerate families of closed periodic orbits in the classical motion.

This very elementary understanding of the origins of shell structure provides a valuable basis for interpreting the qualitative features of shell structure, which we shall now exhibit:

1. Conditions (3.2) and (3.3) provide a classification of the different periods that appear in the fluctuating part of the single-particle level density considered as a function of energy. The simplest periodic orbit corresponds to pendulating motion in which the particle moves back and forth through the center of the spherical potential, $(a, b) = (2 : 1)$, see Fig. 19. The next simplest is the triangular orbit $(3 : 1)$, then more complicated $(4 : 1)$, $(5 : 2)$, etc. For an harmonic oscillator potential, all orbits are planar ellipses with $(a, b) = (2 : 1)$, but for potentials with a more sharply defined surface, as for the nuclear potential, the ratio of radial and angular frequencies is an increasing function of angular momentum (see, for example, the square well potential considered in Fig. 19). In such a potential, the planar figures (triangle, square, etc.) will in the asymptotic limit give many more quantum states than the pendulating orbits $(2 : 1)$ since the degeneracy of the latter involves only two degrees of freedom (the two angles that define the directions of a straight line in space), while the former involves three (for example, the three Euler angles that are necessary to define the relative orientation of two coordinate systems). Thus, we expect the $(3 : 1)$ (triangular) orbits to provide the leading order contribution to the fluctuations in level density at large particle number.

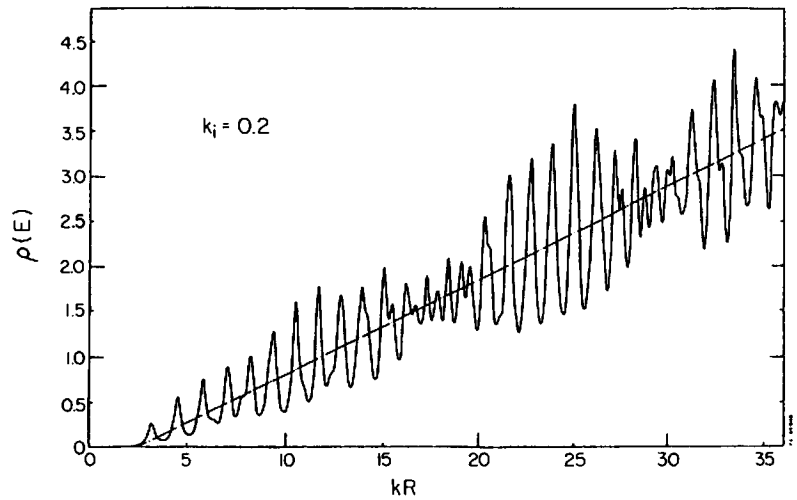

Fig. 20. Quantal level density for single particle in spherical hard wall potential. The discrete eigen values have been given a small Lorenzian width in order to make the level density a continuous function of the wave number. The figure is based on that given by Balian and Bloch [23].

2. The period associated with the triangular orbit in a square well potential is easily estimated:

$$T_\Delta = \frac{3\sqrt{3}\,R}{v_F} \tag{3.5}$$

which implies that the spacing (in wavenumbers k) for the shells associated with the triangular orbits is given by

$$(\Delta k R)_\Delta = \frac{2\pi\hbar}{T_\Delta} = \frac{2\pi}{3\sqrt{3}} \tag{3.6}$$

which is seen to agree very well with the periodicity of the level density oscillations exhibited in Fig. 20. It should be noted that expression (3.5) implies quite generally that the dominant frequency for shell structure oscillations of the single-particle level density are

$$\hbar\omega_{\text{shell}} \sim \frac{\sqrt{\epsilon_F}}{A^{1/3}} \tag{3.7}$$

since the dimensions of the nuclear potential increase with $A^{1/3}$.

3. The number of quantum states associated with a single shell is obtained by estimating the number of values ν in (3.3) that will correspond to approximately

degenerate quantum states; this involves an estimate of the relative importance of the second-order terms in (3.2), which can be obtained from the estimates

$$\frac{\partial\epsilon}{\partial n} \sim \frac{\partial\epsilon}{\partial l} \sim \frac{\epsilon_F}{A^{1/3}}$$
$$\frac{\partial^2\epsilon}{\partial n^2} \sim \frac{\partial^2\epsilon}{\partial n\partial l} \sim \frac{\partial^2\epsilon}{\partial l^2} \sim \frac{\epsilon_F}{A^{2/3}} \tag{3.8}$$

and thus the condition that the second-order contribution to the expansion (3.1) should not spread the energies by more than a fraction of the shell spacing (3.7) implies

$$|\nu| \lesssim \left(\frac{\partial\epsilon}{\partial n}\Big/\frac{\partial^2\epsilon}{\partial n^2}\right)^{1/2} \sim A^{1/6} \tag{3.9}$$

Thus, the total degeneracy for a shell associated with the triangular orbit is

$$g_\Delta \sim \nu(2l+1) \sim A^{1/2} \tag{3.10}$$

which implies a contribution to the level density:

$$\delta\rho_\Delta \sim \frac{g_\Delta}{\hbar\omega_\Delta} \sim \frac{A^{5/6}}{\epsilon_F} \tag{3.11}$$

Note that since the total level density is

$$\rho_{tot} \sim \frac{A}{\epsilon_F} \tag{3.12}$$

the ratio of the triangular oscillation to the total level density (signal-to-noise ratio of the shell structure for large quantum numbers) is

$$\frac{\delta\rho_\Delta}{\rho} \sim A^{-1/6} \tag{3.13}$$

The estimates (3.11) and (3.13) are seen to agree reasonably well with the directly calculated oscillation in the level density exhibited in Fig. 20.

4. The magnitude of the energy advantage of closed shells compared with the average corresponds to the number of states (3.9) being shifted in energy by the amount (3.7), which gives

$$\delta E_{shell} \sim \epsilon_F A^{1/6} \tag{3.14}$$

Thus, the shell effect in the total nuclear energy is very small compared with the bulk terms such as volume ($\sim A$) or surface energy ($\sim A^{2/3}$), but is of the same order as the energy associated with pair correlation and deformation to be considered in later chapters.

5. The striking modulation in the amplitude of the shell structure oscillations exhibited in Fig. 20 can be understood as resulting from the beating of the oscillations associated with the triangle and the square; the difference of these two periods (see Fig. 19) implies

$$\frac{T_\square - T_\Delta}{\overline{T}} = 0.0849 \tag{3.15}$$

corresponding to the observed pattern in which there are about 12 oscillations of the normal shell structure between two maxima or minima of the beating modulations. This interpretation can be directly confirmed by examination of the quantum numbers of the states occurring in the degenerate "bunches" in the regions of the spectrum where the modulation of the shell structure is maximum or minimum (see Fig. 21).

A more detailed derivation of the amplitudes of the shell structure oscillations can be obtained from an asymptotic expansion of the semi-classical expression for the level density [27]:

$$\rho = \sum_\alpha \delta(E - E_\alpha)$$
$$= \sum_{n=\text{integer}} \delta(E - h(\hbar n)) \tag{3.16}$$

where the sum extends over all the eigenvalues E_α of the single-particle Hamiltonian, (h). In the second line of (3.16), the Hamiltonian has been written in terms of the action variable and by semi-classical quantization, the sum over eigenvalues becomes a sum over the integer lattice of the actions

$$I = \hbar n = \hbar(n_1\hat{e}_1 + n_2\hat{e}_2 + n_3\hat{e}_3) \quad (n_1 n_2 n_3) = \text{integers} \tag{3.17}$$

The Poisson summation formula is just constructed to convert the sum of a function over a given lattice into a sum of the Fourier transform of the function over the reciprocal lattice (see [28]); thus, the sum (3.16) becomes

$$\rho(E) = \sum_{m=\text{integer}} \frac{1}{\hbar^3}\int \delta(E - h(I)) \exp\{2\pi i m \cdot I/\hbar\}\, dI \tag{3.18}$$

Of course, the δ functions in (3.18) violate all the analyticity and boundedness conditions that are necessary in order to justify this formula, but we shall, as usual, assume that the δ-functions can be taken as the limit of some well-behaved functions and proceed without scruples. The $m = (0, 0, 0)$ term in (3.18) gives

$$\rho_0(E) = \frac{1}{\hbar^3}\int \delta(E - h(I))\, dI \tag{3.19}$$

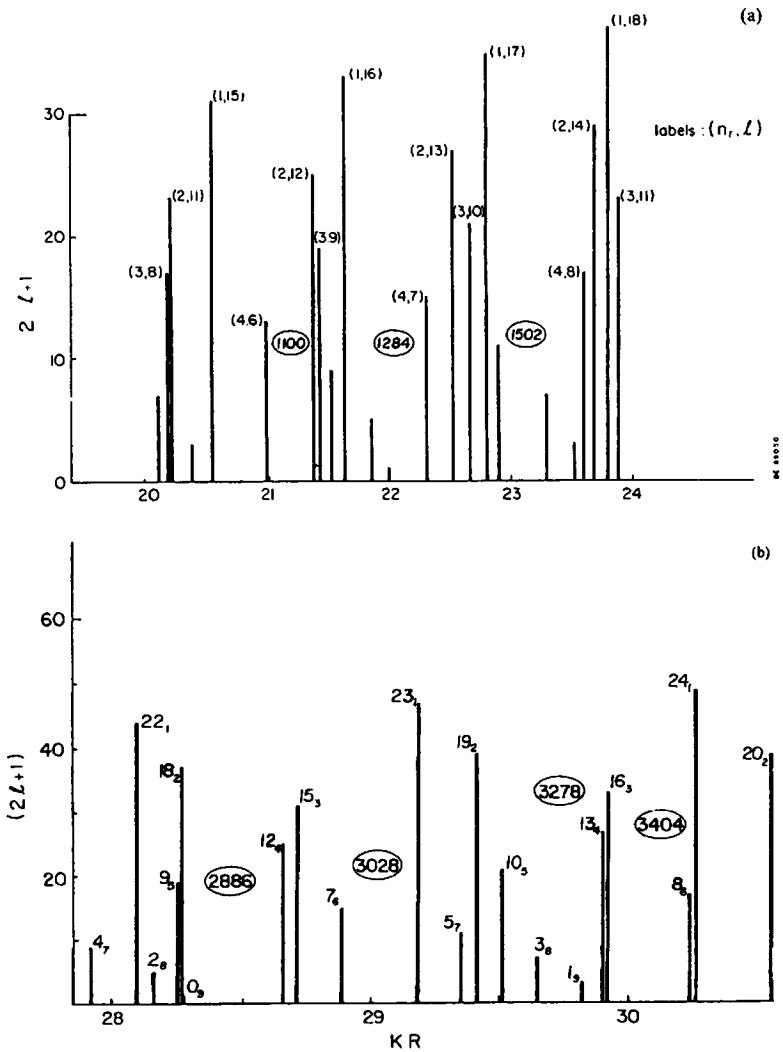

Fig. 21. Details of the single-particle spectrum illustrating the interference between triangular and square orbits in the quantal level density. The n-th eigenvalue with angular momentum, l, is labeled l, n; the height of the stick-figure for each eigen-value is $(2l+1)$, corresponding to the degeneracy of the eigenvalue. Part (a) corresponds to the interval $kR = 20$–24 where triangle ($\Delta l = 3$, $\Delta n = 1$) and square $\Delta l = 4$, $\Delta n = 1$ interfer constructively (compare the strong shell structure oscillations in Fig. 20). Part (b) shows the spectrum for $KR = 28$–31 where it can be seen that the level density maxima for the triangle lie midway between the maxima for the square (i.e. destructive interference).

which is recognized as the Weyl formula for the leading (volume) term in the semi-classical expansion of the average of the level density. The terms with $m \neq (0, 0, 0)$ describe the oscillations.

For large values of the energy, the exponents in (3.18) become large and the integrals can be evaluated by a saddle point approximation. The saddle point is obtained by taking the derivatives of the exponent under the condition that the energy , E, is held constant:

$$\frac{\partial(I \cdot m)}{\partial I_\kappa} - \lambda \frac{\partial h(I)}{\partial I_\kappa} = 0 \tag{3.20}$$

where the second term results from the constraint on the energy. As in (3.4), we recognize the derivative of h with respect to I_κ as the frequency, to obtain

$$\omega_\kappa = \frac{1}{\lambda} m_\kappa \quad m_\kappa = \text{integer}, \tag{3.21}$$

again obtaining the rational ratios of frequencies (closed periodic orbits) as the condition for contributions to the oscillating terms (shell structure) in the nuclear level density. The further evaluation of the saddle point integrals provides the prefactors for the oscillating terms in the level density. The resulting expressions are somewhat complicated and will not be given here; the interested student may consult the original paper by Balian and Bloch (loc. cit.), where the results for a number of standard potentials are given.

Applying the above concepts to the discussion of the shells observed in nuclei, we can see that these are composed of bunches reflecting (2 : 1) and (3 : 1) degeneracies in about equal weight; for example, the shell between $N = 82$ and 126 contains the orbits $(1h_{9/2})(2f_{7/2})(1i_{13/2})(2f_{5/2})(3p_{3/2})$ and $(3p_{1/2})$, (see Fig. 10), which can be interpreted as representing the degeneracy classes

(3 : 1)	$(1i_{13/2})(2f_{7/2})$	22 orbits
(2 : 1)	$(1h_{9/2})(2f_{5/2})(3p_{1/2})$	18 orbits
	$(2f_{7/2})(3p_{3/2})$	12 orbits

where we include orbits in the same periodicity class only if all the orbits have parallel spin and orbit or all the orbits are antiparallel. Thus, we can see that the concepts developed in the present chapter provide a useful language for discussing the shell structure in nuclei, but the asymptotic patterns are only beginning to emerge in the nuclear systems where the particle number is limited to order 100 fermions of each type (see, however, the important role of periodic orbits in understanding the occurrence of super deformation discussed in a later chapter). Remember that even in a nucleus as large as ^{238}U the fraction of nucleons within the distance r_o of the nuclear surface is $3A^{-1/3} \approx 0.5$. In the study of shell structure in metallic

clusters it has been possible to make detailed measurements on systems involving several thousand electrons and in such systems the asymptotic patterns of quantal shell structure are observed in their full glory (see for example Brack [29]).

4. Pairing

In the preceding chapters, we have discussed the interpretation of closed shell structures – the "magic" numbers. In this chapter, we begin the discussion of the structures that are observed for configurations involving particles in partially filled shells. It is important to appreciate that the gaps in the single-particle spectra that create the closed shells imply that the level density within a shell is abnormally high. This high-level density leads to a bewilderingly rapid proliferation in the number of quantum states that should be expected in the low-energy spectrum simply on the basis of the possibilities for distributing a few nucleons among the available orbits provided by the shell model. This feature is illustrated in Table 2, which shows that the shell model configurations involving only two neutrons outside the closed shell ^{208}Pb imply the possibility of fifteen different quantum states below 1 MeV of excitation in the spectrum of ^{210}Pb. When configurations with four or six particles are considered, the number of possibilities increases exponentially with particle number, quickly becoming of order of hundreds or even thousands of expected quantum states with energies within 1 MeV of the lowest state. We cannot avoid a feeling of shock when we compare these expectations with the observed spectra of these nuclei (Fig. 22), which reveal a stunning simplicity and regularity with only two or three levels within the corresponding region of excitation. The challenge that we shall attempt to address in the remainder of this course is to identify and formulate the correlations and associated interactions that select these few favored combinations from among the enormous number of possibilities provided by the shell model. These problems are of a similar nature to those encountered in atomic structure and in the fractional quantum Hall effect, where degeneracies in configurations with partially filled shells open the possibility for

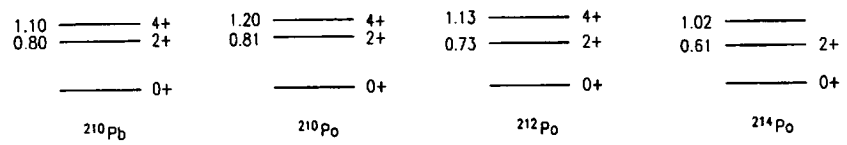

Fig. 22. The experimentally observed spectra of the nuclei analyzed in Table 2. The means of excitation available in these experiments, as well as the systematics of the spectra of other similar nuclei provide considerable confidence that no states below 1 MeV have been missed in the spectra.

Table 2

Enumeration of quantum states expected for low lying configurations in the neighborhood of ^{208}Pb

Nucleus	Config	$E - E_0$ (MeV)	Quantum states (I)	# states $E - E_0 \leq 1$ Mev
^{210}Pb	$g_{9/2}^2$	0	0 2 4 6 8	15
	$g_{9/2}\, i_{11/2}$	0.78	1 2 3 4 5 6 7 8 9 10	
^{210}Po	$h_{9/2}^2$	0	0 2 4 6 8	13
	$h_{9/2}\, f_{7/2}$	0.89	1 2 3 4 5 6 7 8	
^{212}Pb	$g_{9/2}^4$	0	$0^2\ 2^2\ 3\ 4^3\ 5\ 6^3\ 7\ 8^2\ 9\ 10\ 12$	116
	$g_{9/2}^3\, i_{11/2}$	0.78	$0\ 1^4\ 2^6\ 3^8\ 4^9\ 5^{10}\ 6^{10}\ 7^{10}\ 8^9$ $9^8\ 10^7\ 11^5\ 12^4\ 13^3\ 14^2\ 15\ 16$	
^{212}Po	$(g_{9/2}^2)_n\ (h_{9/2}^2)_p$	0	145 states	775
	$(g_{9/2}\, i_{11/2})_n\ (h_{9/2}^2)_p$	0.78	350 states	
	$(g_{9/2}^2)_n\ (h_{9/2} f_{7/2})_p$	0.89	260 states	
^{214}Po	$(g_{9/2}^4)_n\ (h_{9/2}^2)_p$	0	606 states	5402
	$(g_{9/2}^3\, i_{11/2})_n\ (h_{9/2}^2)_p$	0.78	3706 states	
	$(g_{9/2}^4)_n\ (h_{9/2}\, f_{7/2})_p$	0.89	1090 states	

The table is intended to indicate the level density in the neighborhood of the ground state that is expected on the basis of an independent particle description involving a few particles outside the closed shell configuration of ^{208}Pb. The lowest available single particle configurations are listed in column two and their zero order energies (as obtained from the one particle spectra in Fig. 11) are given in column three (the table only includes configurations with energies less than 1 MeV). The expected values of the total angular momentum, I, resulting from these configurations (with due account of the Pauli principle for identical particles) is given in column four. Multiplicity in the occurrence of a given value of I is indicated by an exponent. The total number of quantum states within 1 Mev of the ground state on the basis of this enumeration is given in column five.

correlations that stabilize new structures. However, nuclear correlations differ in a major way from those encountered in atoms and the Hall effect problem as a result of the fact that the effective interactions in the latter problems derive from the repulsive Coulomb forces and thus the interpretation of the lowest states in these problems involves an analysis of how to construct wave functions in which the valence electrons are kept as far away from each other as possible within the restriction imposed by the requirement that one uses only configurations of the valence shell. In nuclei the residual interactions are dominantly short range and attractive and so we must try to find structures that cause the valence nucleons to overlap with each other as much as possible (again with the restriction that these structures be built out of the available valence configurations). From the analyses of nuclear spectra, two different mechanisms have been found to play important and competing roles in exploiting the possibilities resulting from the shell model

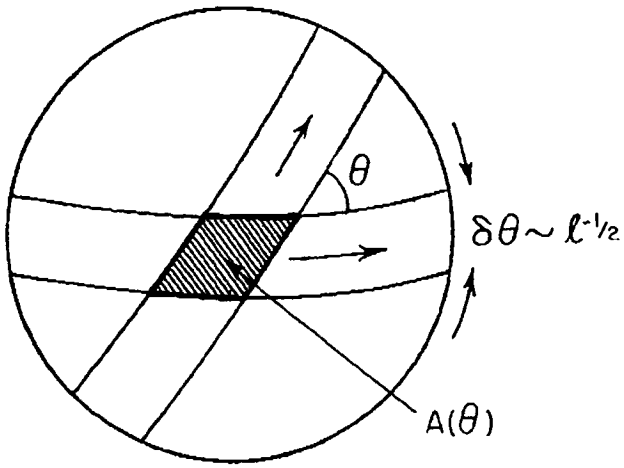

Fig. 23. Semi-classical analysis of the expectation value of a short-ranged interaction between two particles each with angular momentum, l. The semi-classical picture of a single particle with angular momentum, l, implies confinement to the neighborhood of the plane perpendicular to the direction of l. The angular width of the confinement is obtained from the wave function $Y_{ll}(\theta\phi)$ which yields $\delta\theta \sim l^{-1/2}$. If the two particles are coupled together to a total angular momentum, L, the angle between the two orbital planes is $\Theta = \cos^{-1}[\frac{1}{2}(L/l)^2 - 1]$ and the overlap of the two densities is proportional to the shaded rectangle.

degeneracies: pair correlations and collective shape deformation of the mean field. In this chapter, we shall first address the issues connected with pair correlations.

In order to get started with the problem of thinking about how to build efficient correlations in many-body shell model wave functions, it is useful to consider a configuration of just two particles moving in a single-particle orbit. For simplicity, we shall ignore the spin orbit force, and consider an orbit with orbital angular momentum $l \gg 1$, so that we may think in semi-classical terms. The classical picture would confine the motion to the equatorial plane perpendicular to the direction of the angular momentum, l, but the quantal uncertainty implies an angular fuzziness of order $l^{-1/2}$ about this plane. We shall explore the effect of a short-range (δ-function) attractive force acting in configurations of (identical) fermions moving in such an orbit. For two particles (l^2), the exclusion principle forces us to consider only the spin singlet states with total orbital angular momentum, $L = 0, 2, \ldots, 2l$, since the spin triplet odd L values are spatially anti-symmetric and the δ-function attraction vanishes. The simple picture of the quantum orbit suggests that we consider the short-range interaction between the two particles in terms of the overlap of the two orbits as in Fig. 23, which leads to the semi-classical estimate of the interaction sketched in Fig. 24. The proper quantal calculation of the matrix element of a δ-function can be carried out by expanding the δ-function in spherical harmonics and recoupling the angular momenta to yield

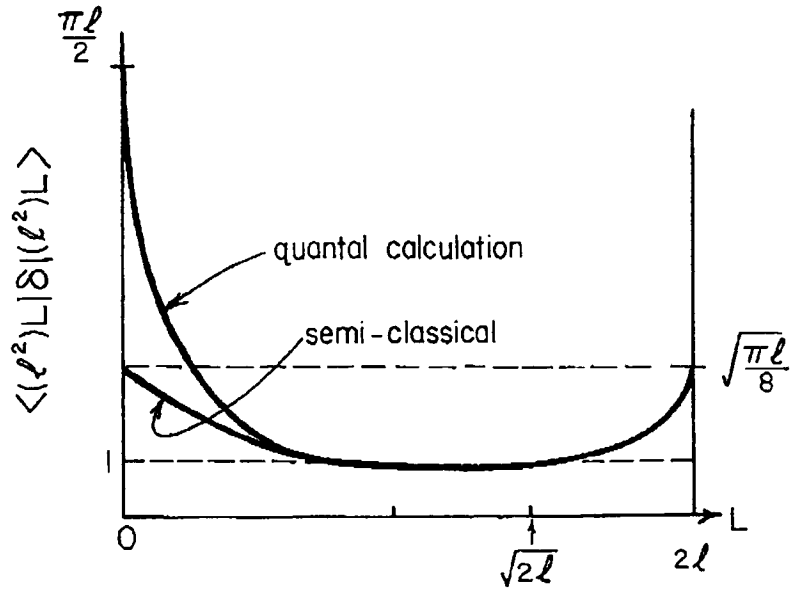

Fig. 24. Comparison of semi-classical and quantal evaluation of short-ranged interaction in configurations $(l^2)L$.

$$\langle {}^1L(l^2)|\delta(r)|{}^1L(l^2)\rangle = \mathcal{R}(2l+1)\langle l0, L0|l0\rangle^2 \tag{4.1}$$

where $\mathcal{R}$ is a (positive) radial integral and the last factor is the vector addition coefficient that results from the recoupling of angular momenta. The expression (4.1) is plotted in Fig. 24 and compared with the semi-classical estimate described above and in Fig. 23. It is seen that the semi-classical picture does very well for $L \gg 1$, but fails disastrously for $L = 0$. In fact, the short-range correlation between the two particles in the state $(l^2)_{L=0}$ is a factor $\sqrt{l}$ greater than would have been expected from the fuzziness of the individual orbits, and represents a collective effect in the $L = 0$ wave function which is built up as a coherent superposition of all $2l + 1$ different m-components of a particle moving in an orbit with angular momentum l. The remarkable short-range correlation in the $L = 0$ state can be seen directly in the wave function by recognizing that the

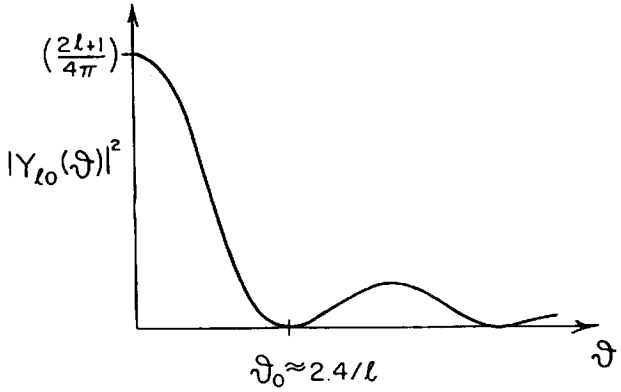

Fig. 25. Probability distribution for the relative angle between two particles in the quantal state $(l^2)_{L=0}$. From the wave function (4.2) and the well-known asymptotic expression $P_l(\Theta) \sim J_0(l\Theta)$, $l \gg 1$ we obtain the probability distribution as sketched.

vector coupling of the two angular functions yields

$$\psi(l^2; L) = \sum Y_{l\mu}(\theta_1\phi_1) Y_{l-\mu}(\theta_2\phi_2) \langle l\mu, l-\mu | L0\rangle$$

$$\psi(l^2; L=0) = \frac{1}{\sqrt{2l+1}} \sum Y_{l\mu}(\theta_1\phi_1) Y_{l-\mu}(\theta_2\phi_2)(-)^{l-\mu}$$

$$= \frac{1}{\sqrt{4\pi}} Y_{l0}(\theta_{12}) \tag{4.2}$$

where θ_{12} is the angle between the position vectors of the two particles. The well-known features of the spherical harmonic Y_{l0}, plotted in Fig. 25, confirms the remarkably strong angular correlation of the two particles, extending over angles of order $\theta_{12} \lesssim l^{-1}$. This correlation is a unique feature of the $L = 0$ state and the δ-interaction as given in (4.1) is reduced by a factor of 4 already for the $L = 2$ state (see Fig. 25).

If we had considered $(j^2)_J$ states in the above example (i.e. treating spin–orbit coupled states as is more appropriate in nuclear configurations), the factor $(2l + 1)\langle l0\, L0 \,|\, l0\rangle^2$ in (4.1) would be replaced by $(j + 1/2)\langle j\, 1/2\, J0 \,|\, j\, 1/2\rangle^2$, which has exactly the same spectral pattern as in Figs. 24 and 26 with a strong attraction in the $J = 0$ state which is already reduced by a factor of 4 in the first excited $J = 2$ state.

If there had been two degenerate single-particle orbits, j_1 and j_2, the attractive

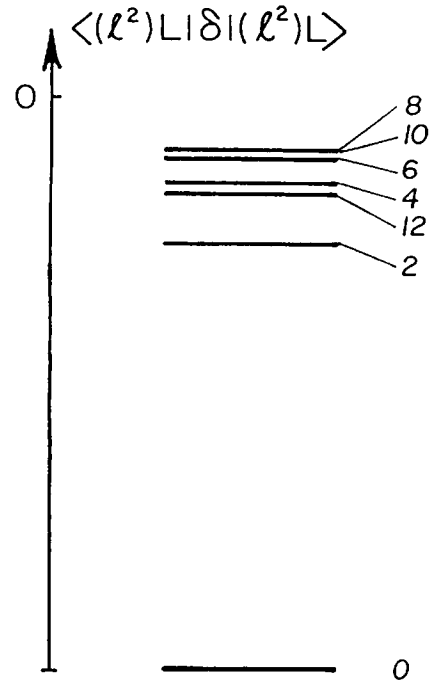

Fig. 26. Spectrum for configuration $(l^2)_L$ with δ-function interaction and $l = 6$.

δ-function produces a lowest state

$$|\,\rangle = \frac{1}{\sqrt{\Omega}} \left\{ \sqrt{j_1 + 1/2}\, |(j_1^2)_{J=0}\rangle + \sqrt{j_2 + 1/2}\, |(j_2^2)_{J=0}\rangle \right\}$$

$$\Omega = (j_1 + 1/2) + (j_2 + 1/2) \tag{4.3}$$

assuming that all the radial integrals are equal. In this state, the angular correlation of the particles is still further increased; the angular separation becoming

$$\delta\theta_{12} \lesssim (j_1 + j_2)^{-1} \tag{4.4}$$

We see in (4.3) a further development of the correlation effect recognized in (4.2); the short-range attraction attempts to build a wave packet in which the available single-particle states (jm) are paired with their unique partner related by time reversal $(j\bar{m})$, and these pairwise occupied states are linearly superposed with equal weights to produce the highly correlated $J = 0$ state. A convenient effective

interaction which does exactly this job can be written

$$V_p = -G\,A^+\,A$$

$$A = \sum_{\nu>o} a_{\bar{\nu}} a_\nu$$

$$A^+ = \sum_{\nu>o} a_\nu^+ a_{\bar{\nu}}^+ \tag{4.5}$$

where in a spherical potential the states ν may be labeled by (jm) and $\bar{\nu}$ is the state related to ν by time reversal; the coupling constant G measures the strength of the effective short-range attraction.

In general, the single-particle orbits within a shell are not all degenerate and so in building the two-particle pair correlation, we should include the effect of the single-particle energies against which the pairing interaction, V_p, must compete:

$$\mathrm{H} = \sum \epsilon_\nu (a_\nu^+ a_\nu + a_{\bar{\nu}}^+ a_{\bar{\nu}}) + V_p \tag{4.6}$$

The spectrum of ^{206}Pb provides a simple example in which the correlated two-particle state described above can be worked out in detail and compared with experimental data. The energies $\epsilon(j)$ and degeneracies of the single-particle orbits, j, can be taken from the observed spectrum of ^{207}Pb (single hole states) (see Fig. 11). The Hamiltonian (4.6) implies that the ground state eigenvalue, E_o, is obtained as the lowest energy solution to the equation

$$G \sum \frac{(j+1/2)}{2\epsilon(j) - E_o} = 1 \tag{4.7}$$

The observed ground state energy is

$$E_o = -0.64\ \mathrm{MeV} \tag{4.8}$$

measured with respect to the energy of the lowest shell model configuration $(p_{1/2}^{-2})$. From (4.6) and (4.7) and the energies in Table 2, the coupling constant G can be determined:

$$G = 0.14\ \mathrm{MeV} \tag{4.9}$$

This value agrees well with the systematics ($G = 25$ MeV/A) obtained from measurements of binding energies and wave functions of many other nuclei in the range $60 < A < 250$. With all the parameters in the Hamiltonian (4.6) now determined, the amplitudes $c(j)$ in the wave function

$$|\,^{206}\mathrm{Pb}(0)\rangle = \sum_j c(j)\,|(j^{-2})_o\rangle \tag{4.10}$$

Table 3

Theory and observation of the structure of the correlated ground state of ^{206}Pb

orb(j)	$g(j)$	$E(j) - E(p_{1/2})$	$(c(j))_{calc}$	$(c(j))_{exp}$
$p_{1/2}$	1	0	0.74	0.66
$f_{5/2}$	3	0.57	0.46	0.51
$p_{3/2}$	2	0.89	0.28	0.32
$i_{13/2}$	7	1.63	0.32	0.28
$f_{7/2}$	4	2.34	0.18	0.22
$h_{9/2}$	5	3.47	0.14	0.3

can be obtained from the relations

$$c(j) = \frac{GM\sqrt{j+1/2}}{2\epsilon(j) - E_o} \tag{4.11}$$

$$M = \left\{ G^2 \sum \left(\frac{\sqrt{j+1/2}}{2\epsilon(j) - E_o} \right)^2 \right\}^{-1/2} \tag{4.12}$$

These calculated amplitudes are given in the 4th column of Table 3 and can be compared with the experimentally observed amplitudes listed in column 5. The amplitudes have been determined from experimental cross-sections for the reaction ^{206}Pb(dp)^{207}Pb populating the single- particle states in ^{207}Pb; the absolute values of these cross-sections can then be compared with single-particle values obtained from the inverse (one-particle pick-up) reaction ^{208}Pb(pd)^{207}Pb populating the same states in ^{207}Pb. The magnitude of the pair correlation produced by the pairing force (4.5) is measured by M^2 as given by (4.11); in the absence of a pairing interaction, the ground state of ^{206}Pb would be described by the single configuration $c(p1/2) = 1$ which yields $M^2 = 1$, while the amplitudes listed in Table 3 imply $M^2 = 12.0$. This correlation of the two neutrons (holes) in the ^{206}Pb-ground state is also directly seen as a strong enhancement of the two-particle pick-up reaction ^{208}Pb(pt)^{206}Pb(0).

We have so far only considered the pair-correlated state for two particles, but our real interest is in the correlations for configurations involving many particles. So we go back to our simple degenerate problem with particles in a single orbit with angular momentum, l, and consider configurations with 3, 4, 5, ... particles. If the first two particles occupy the correlated state (4.2), the spherical symmetry of this state makes it impossible for a third particle to establish correlations with either of these original particles without disrupting their elegant correlation; in this situation, the lowest energy state for the (l^3) is one in which the odd particle occupies one of the (lm) states and the original pair preserves its correlation (as